AD-772 867

EXPLOSIVE TECHNIQUES FOR HIGH ALTITUDE METAL RELEASES

Robert A. Fluegge

Calspan Corporation

Prepared for:

Rome Air Development Center
Defense Advanced Research Projects Agency

August 1973

RADC-TR-73-307
Final Technical Report
August 1973

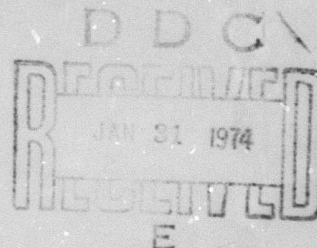EXPLOSIVE TECHNIQUES FOR HIGH ALTITUDE METAL RELEASES

CALSPAN CORPORATION

Sponsored by
Defense Advanced Research Projects Agency
ARPA Order No. 1649

Approved for public release. Distribution unlimited.

The views and conclusions contained in this document are those
of the authors and should not be interpreted as necessarily
representing the official policies, either expressed or implied,
of the Defense Advanced Research Projects Agency or the U. S.
Government.

Rome Air Development Center
Air Force Systems Command
Griffiss Air Force Base, New York

AD772867

REPORT DOCUMENTATION PAGE		READ INSTRUCTIONS BEFORE COMPLETING FORM
1. REPORT NUMBER RADC-TR-73-307	2. GOVT ACCESSION NO.	3. RECIPIENT'S CATALOG NUMBER
4. TITLE (and Subtitle) Explosive Techniques for High Altitude Metal Releases		5. TYPE OF REPORT & PERIOD COVERED Final 1 Jan 73-1 Jun 73
		6. PERFORMING ORG. REPORT NUMBER
7. AUTHOR(s) Mr. Robert A. Fluegge		8. CONTRACT OR GRANT NUMBER(s) F30602-72-C-0436
9. PERFORMING ORGANIZATION NAME AND ADDRESS CALSPAN Corp P. O. Box 235 Buffalo, NY 14221		10. PROGRAM ELEMENT, PROJECT, TASK AREA & WORK UNIT NUMBERS PE - 62301E Wun - 05 Proj - 1649 Task - 02
11. CONTROLLING OFFICE NAME AND ADDRESS Advanced Research Project Agency 1400 Wilson Blvd Arlington, VA 22209		12. REPORT DATE August 1973
		13. NUMBER OF PAGES 41
14. MONITORING AGENCY NAME & ADDRESS(If different from Controlling Office) RADC (OCSE/J. Simons) Griffiss AFB, NY 13441		15. SECURITY CLASS. (of this report) UNCLASSIFIED
		15a. DECLASSIFICATION/DOWNGRADING SCHEDULE

16. DISTRIBUTION STATEMENT (of this Report)

Approved for public release. Distribution unlimited.

17. DISTRIBUTION STATEMENT (of the abstract entered in Block 20, if different from Report)

18. SUPPLEMENTARY NOTES

19. KEY WORDS (Continue on reverse side if necessary and identify by block number)

iron
vaporization
shock heating
equation-of-state
metals

20. ABSTRACT (Continue on reverse side if necessary and identify by block number)

Shock heating techniques have been developed and used to cause vaporization in porous iron samples. The effects of iron porosity, explosive configuration and type, and energy coupling techniques were investigated. The overall goal is to cause sufficient vaporization such that dense clouds of Fe atoms can be generated.
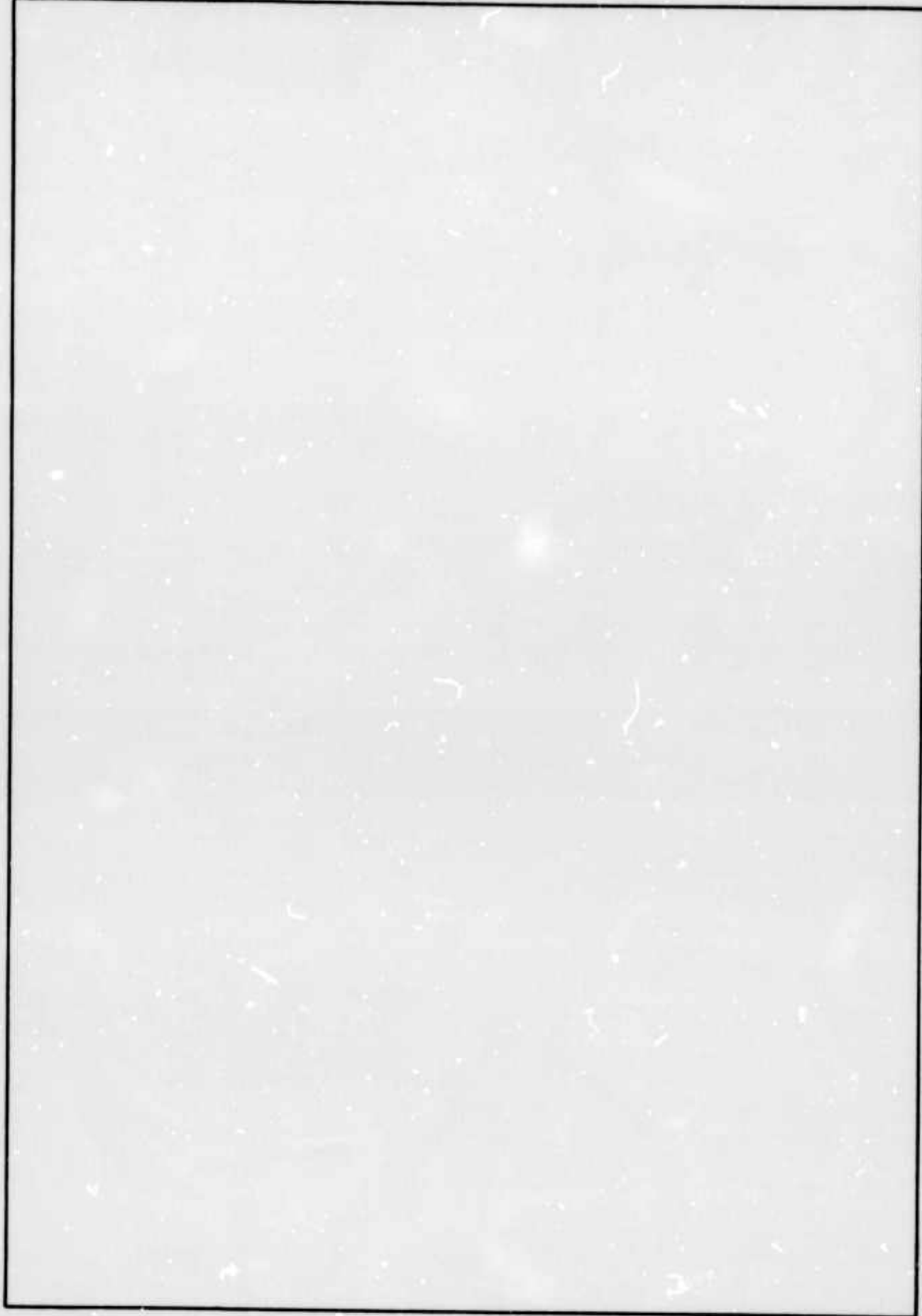
DD FORM 1 JAN 73 1473   EDITION OF 1 NOV 65 IS OBSOLETE

i

EXPLOSIVE TECHNIQUES FOR HIGH ALTITUDE METAL RELEASES

Robert A. Fluegge

ia

PUBLICATION REVIEW

This technical report has been reviewed and is approved

RADC Project Engineer

FOREWORD

TABLE OF CONTENTS

GLOSSARY OF ABBREVIATIONS AND ACRONYMS

PBX-9404	-	94% HMX plus 6% Binder - Explosive
PBXN-5	-	95% HMX plus 5% Viton Binder - Explosive
M. P. I.	-	Max Planck Institut
EG&G	-	Trade name of EG&G Corporation
PBX-9407	-	94% RDX plus 6% Exon Binder - Explosive
EXTEX 8003	-	80% PETN plus 20% Silicone Rubber - Explosive
A. E. C.	-	Atomic Energy Commission
EBW	-	Exploding Bridge Wire
H. E.	-	High Explosive
TNT	-	Trinitrotoluene

LIST OF ILLUSTRATIONS

Section 1

INTRODUCTION

The use of explosives was studied during this program as a technique for achieving vaporization and the release of free metal atoms. The energy release rate and total energy per unit mass is very high for many commercially available explosives. As a comparison, the power density from an acetylene flame is approximately 10^2 watts cm^{-3}, while that from high explosives is approximately 10^{10} watts cm^{-3}.[1] Two principal methods have been utilized to transfer explosive energy to the material to be vaporized, i.e., the target material------the contact method and the collision method. Both methods incorporate techniques to pass high energy shock waves through their targets; this increases entropy of the target and hence its temperature. The increased heat content causes partial vaporization of the metal.

In the contact method, the metal to be heated is placed on the outside, but in direct contact with the explosive. The detonation shock from the explosive passes into the metal, with the pressure levels and efficiency of energy transfer governed principally by the shock impedance match of the explosive/metal system. For the case of a highly efficient explosive such as PBX 9404 with a density of 1.82 g/cc and iron at normal crystalline density, a pressure level of approximately 500 kilobars[2] can be achieved in iron. The "shock" temperature in the iron would be slightly less than 800°K which would subsequently decay rapidly to under 600°K with passage of the shock[2]. This iron temperature is too low for large scale vaporization to occur. Increasing the amount of explosive with respect to the target mass will not produce an increase in entropy (or peak temperature) in the target with the contact method, although the temperature decay time profile could be altered slightly. Hence, the direct contact method using normal density iron would not be expected to produce sizable clouds of free iron atoms.

One way to increase entropy in the metal is to significantly lower the initial compaction or density of the material to be heated significantly below normal crystalline densities. Upon passage of a shock, a substantial amount of work is expended in irreversibly crushing the voids between particles. The

1

large change in specific volume occurring on compression is not reversed as the shock passes and the material isentropically unloads (expands) due to exposure to a hard vacuum. The residual energy appears as internal energy producing higher peak temperatures in the porous target material than found in materials with normal crystalline densities.

The collision method separates the material to be heated from the explosive. Use of the collision method usually permits greater energy transfer to target materials than found in the direct contact method. This method employs a "flyer plate" launched by a detonating explosive. After travelling a short distance, this plate collides with the target, producing shock waves which pass through both flyer and target. The flyer plate velocity is a function of explosive charge-to-plate mass ratio; plate velocities approximately four times those of the maximum particle velocities achievable with high energy explosives in the direct contact methods can be produced. For example, an iron plate traveling at 4 km/sec impacting on an iron target will produce pressures of approximately one megabar in crystalline density iron.[3] This in turn would produce a peak temperature of approximately 2000°K, which relaxes to approximately 1100°K after shock passage. Using flyer plates made of materials with higher shock impedences than iron (such as the tantalum used here) significantly increases target plate entropy and peak temperatures for a given impact velocity.

An alternative direct contact technique could employ a uniform dispersion of metal particles in the explosive. Considering the shock heating phenomena only, the method is equivalent to the direct contact technique discussed above. However, the residence time of the particles in the reaction zone could likely permit the attainment of temperatures approaching those of the detonation temperature of the explosive. Chapman-Jouguet (C-J) temperatures for two military explosives which are major constituents of the plastic bonded explosives used in these experiments are listed in Table I. The highest density is approximately the maximum achievable. The lowest value approaches a minimum stable compaction. Temperatures near 3000°K appear to be achievable.

Table 1

Detonation Temperature for HMX and RDX in °Kelvin[4]

Density in g/cc

	1.0	1.4	1.6	1.8	1.9
HMX	3587	3258	2955		2364°K
RDX	2588	3272	2970	2588°K	

Metal loadings of up to 25% total weight can probably be used. This would be a significant gain in reducing charge-to-mass ratios over the equivalent flyer plate system. For example, a charge to flyer mass ratio of approximately 9 to 1 is required to achieve flyer plate velocities which produce equivalent temperatures in porous iron. It must be remembered, however, that the attainment of near equilibrium temperatures with the in situ metal/ explosive system is highly speculative and remains to be experimentally verified.

Other variations of the above techniques are possible for increasing pressures and temperatures in target materials. These could employ the principles of shock wave interaction such as the formation of Mach stems or stagnation zones.

The choice of testing the flying plate techniques in the present studies was based on the success of similar work at the Max Planck Institut (M.P.I.), in Germany and the need for producing large increases of entropy in the target. This was especially true for iron due to its relatively high melting (2200°K) and boiling (3300°K) temperatures. Twenty-two experiments were performed in the course of these studies to determine the effects of explosive composition and configuration, flyer plate thickness and velocity, and target porosity on iron vaporization. Analytical models were also investigated to show vaporization trends as these parameters are varied.

Section 2

EXPERIMENTAL METHOD

The present experiments were performed in the Calspan high altitude test chamber shown in Figure 1; it is 4 m in diameter and 12.2 m long and made of 1.3 cm thick steel which is covered with a low vapor pressure epoxy. The chamber was routinely evacuated to pressures near 2×10^{-5} torr using the 36 inch oil diffusion pump and two high volume Roots blowers. The flyer plate launch assembly and iron target plate are located at one end of the chamber, and the various diagnostic instrumentation are deployed downstream of the metal target release point.

High speed photography was used to obtain the relationship between axial and radial velocities in the expanding jet. At a preset time after flyer plate impact on the iron target plate, an EG&G Flash lamp is triggered and produces about 50 million candle power with a 1.5 μsec duration time. A shadow is obtained on a translucent, Mylar screen; the shadow is caused by light absorption and scattering due to the particulate and gaseous material in the flow field. Knowing the exact release time, and the time at which the shadowgraph was taken, enables calculation of the radial and axial velocity components.

A 1/2-meter Jarrell-Ash monochrometer and a 1000 watt Xenon arc lamp are located 231 cm downstream of the flyer plate assembly. The arc lamp acts as a broad band reference light source, and the monochrometer is used to measure absorption due to atomic and particulate matter. The integrated absorption over a pressure broadened atomic iron line can be related to the line-of-sight densities between the arc lamp and the monochrometer. The 3719.94 Å line in iron was used. For atom densities in the 10^{14} to 10^{16} cm^{-3} range, the absorption line width is proportional to the atomic concentrations and ranges between a few tenths to several angstroms. As a best compromise, a monochrometer resolution of 3.0 Å was used in these experiments.

Three photomultipliers on the output of the Jarrell-Ash monochrometer were used to record the light scattering/absorption due to particulate and gaseous species. Each photomultiplier output was monitored in real time on dual beam oscilloscopes that were triggered and timed to start recording data upon H. E. detonation.

Several high energy fragment shields were located within the confines of the chamber. These were constructed of 3/4 inch thick steel plates located so as to stop direct impact of the released material on the chamber walls. The shields became heavily pitted, but contained the explosive releases throughout the program.

The experimental system is illustrated in the block diagram shown in Figure 2. The fire switch at the right is used to control the High Explosive (H. E.) detonator, the high speed camera, the EG&G flash lamp and the trigger inputs to the dual beam recording oscilloscopes. A Cordin high energy pulser was used to rapidly trigger the several detonators tested during this program. It supplies a 5000 volt pulse, having a rise time of 0.3 microseconds. This fast rise pulse coupled with the fast acting detonator and H. E. cause the flyer plate to be launched and reach maximum speed within a few microseconds.

Two specially designed timing pins were used to determine flyer plate velocities. They were shorting-pin type units that resulted in two pulses that are a measure of the time it takes the flyer plate to travel a fixed distance. These signals were also used to predict more exactly the time of flyer plate impact upon the iron targets.

Two photodiodes (EG&G) were used to monitor the exact time at which the H. E. detonation and the EG&G flash lamp signals occurred. The signal from each photodiode was recorded using dual beam oscilloscopes. Each oscilloscope could be triggered only once, and its recording start-point was controlled by the fire switch shown in Figure 2.

2.1 CALSPAN FLYER PLATE LAUNCH ASSEMBLY

A flyer plate launch assembly that would produce high plate velocities, and could simultaneously be scaled to larger sizes was designed, fabricated and tested during this program. The system is shown in Figure 3.

The heart of the system is the distributor plate, fabricated of Lexan polycarbonate plastic and shown as callout 3 in the figure. A series of grooves in the plate provided a distribution network for transferring the detonation from a single point input to a 12 point simultaneous output. This network is extrusion loaded with Extex 8003, an 80% PETN - 20% silicone elastomer bonded explosive. The plate also contained strategically placed void grooves to attenuate cross channel shocks which tend to degrade system performance. Test fire results for one of these plates are listed in Table II. These were obtained from streak camera records by Mason & Hanger-Silas Mason Company, operators of the Burlington A.E.C. Plant and fabricators of the plates. The detonator used for this test was an EX12B EBW type. The measured standard deviation of 41 nanoseconds for the 12 points appears to be more than adequate and is conservative from a design limitation.

The detonator compatible with this design and normally used at Calspan was a Reynolds RP-87 EBW type. Use of larger detonators could result in point drop-out due to shock interference, or out of phase emergence due to decaying velocity in the distributor network. The Reynolds RP-87 detonator is recommended for safety and timing considerations at reasonable cost.

The simultaneous detonations from the twelve discrete output points initiates and spreads in the PBX-9407 booster pellet. PBX-9407 is composed of 94% RDX bonded with 6% Exon 461 plastic and has a steady-state detonation velocity of 7.9 km/sec.[5] at 1.60 g/cc density. It provides a smooth transition of the detonation from the distributor plate to the main charge.

Two different HMX based main output charges were used in these experiments; they were PBXN-5 and PBX 9404. The PBXN-5 is a Navy-type approved explosive consisting of 95% HMX and 5% Viton elastomer binder. The PBX 9404 is composed of 94% HMX with 6% binder consisting of equal parts of nitrocellulose and tris-β-chloro-ethylphosphate. The two explosives

Table II
DISTRIBUTOR PLATE TIMING SEQUENCE FOR
EACH OF THE 12 POINT DETONATIONS

Point Number	Time to Detonate μsec
1	2.578
2	2.537
3	2.552
4	2.576
5	2.572
6	2.582
7	2.574
8	2.524
9	2.490
10	2.571
11	2.478
12	2.473

Average Transit Time: 2.542 μsec

Maximum Spread - Fastest to Slower Points: 0.109 μsec

Standard Deviation - 12 points: 0.041 μsec

Detonator Timing: 2.622 μsec

Piece Temperature: 56°F

have nearly equal detonation velocities of approximately 8.8 km/sec.[5] at 1.84 g/cc. PBX 9404 is particularly well known as an excellent metal accelerator.[6]

As the detonation expands laterally from the discrete initiation points shock interaction will occur on lines equidistant from neighboring points, producing high pressures and locally high velocities. In a properly designed multi-point system, these local discontinuities will not become unstable, but will aid rapid buildup of the primary shock front to steady state conditions. The output from the main charge is essentially a steady-state plane wave. This plane wave drives the flyer plate intact to the target.

Several experiments were performed during this program with the H.E. assembly simply mounted in free space and aligned to cause direct and uniform flyer plate impact on the iron targets. Since flyer plate velocity can be increased by confining the explosive charge, an enclosed configuration shown in Figure 4 was also tested. In this configuration, the high explosive is confined in a thick steel enclosure which essentially cannot move until the flyer plate is launched and on its way toward the iron target. The metal holder was completely destroyed during each test. The largest fragments were about 1/2-inch in diameter, and most of the holder appeared as smaller pieces scattered about the test chamber.

Based on Gurney calculations,[7] velocity enhancement of about 9% would be expected for the 9.5 to 1 charge-to-mass (C/M) ratio used here. Confinement is much more effective at lower C/M ratios, although net or final velocities are reduced. At unity C/M ratios a 60% velocity increase is indicated[7] for confined charges over the open-sandwich model. Experimental results at Calspan tend to support these calculations, and an improved metal vaporization efficiency was measured.

Design considerations for future experiments could include a spherically shaped charge and flyer plate to further increase plate velocities and subsequent vaporization. The spherical shape would approximate a uniformly confined configuration.

2.2 MAX PLANCK INSTITUT FLYER PLATE ASSEMBLY

The flyer plate assembly designed and used at both M.P.I. and in this program is shown in Figure 5. A Swiss-made detonator, sold under the trade name Euratom, was incorporated to trigger the H.E. It is a hot wire type similar to U.S. #8 strength electric blasting caps. A tetryl booster and specially refined castable H.E. composed of 85% RDX and 15% TNT was used as the main charge. The units were made by the Messerschmit-Bolkow-Blohm Corporation, Germany. They are identical to those previously tested at M.P.I. [8,9] A thin (0.003 in.) polyacetate film and a tantalum flyer plate were cemented to each other and directly onto the main explosive.

Two shorting wire type pins for timing the arrival of the flyer plate are shown located just outside the steel shield which was used to partially confine the detonation products. The ends of these timing pins were 1.3 cm apart, and typical timing between successive pulses was between 2 and 3 microseconds. The complete assembly is destroyed in each experiment.

The porous iron target plate shown at the far left in Figure 5 was cemented in place as in the Calspan design. Iron plates having porosities ranging between 58% and normal crystalline densities were shock heated and tested. Basically this configuration and the Calspan design are very similar, but the Calspan design should be more accurately scalable to larger payloads. It would be relatively simple to incorporate more than 12 points in the distributor plate in a larger Calspan design, and would be more volumetrically efficient.

Section 3

VAPORIZATION

The number of free iron atoms that are released as a result of shock heating was determined by atomic absorption spectroscopy. Since the expected concentrations were high, resonant-line shape was dominated by pressure broadening; a computer program was used to calculate the expected line shapes. The absorption was calculated by integrating over these line shapes and then compared to measured absorption signals. The comparison enables the determination of the centerline free atom densities in the high altitude test chamber at any given time.

The flow field contains solid, liquid, and gaseous particles. To distinguish between the number of free iron atoms and particles, the absorption in three wavelength regions was measured and compared to each other. The gas phase absorption by iron was monitored at $3719.94 \pm 1.5 \, \overset{\circ}{A}$ which corresponds to the transition between the $^5D_4$ ground state and its $^5F_5$ upper state. The measured oscillator strength for this line is reported by Huber and Parkinson[10] to be 0.041. Signals resulting from scattering due to particulates were monitored at $3710 \pm 10 \, \overset{\circ}{A}$ and $3730 \pm 10 \, \overset{\circ}{A}$ to bracket the resonant iron absorption line. The signal differences between continuous and resonant absorption were used to determine the number of iron atoms in the light path.

The number of atoms, n, in a symmetric jet of radius Y_B and of length dx at a given time is given by:

$$\frac{dn}{dx} = \int_0^{Y_B} \rho \, 2\pi y \, dy \qquad (1)$$

where: ρ = atomic densities.

The atom and particulate velocities are assumed equal, constant in time, and originating from a point source. Thus flow velocities are given by

$$\dot{X} = \frac{X}{t} \quad \text{and} \quad \dot{Y} = \frac{Y}{t} \qquad (2)$$

10

and the gas density distribution can be described by [8,9]

$$\rho = \rho_{\mathfrak{c}} \cos^{m} \left(\frac{\pi}{2} \frac{y}{Y_B} \right)$$

(3)

where: $\rho_{\mathfrak{c}}$ = symmetric jet centerline density
m = constant; taken to be 2 based on the experience at M. P. I.

Substituting equation 3 into 1 gives

$$\frac{dn}{dx} = 2 \pi \rho_{\mathfrak{c}} \int_{o}^{Y_B} y \cos^{2} \left(\frac{\pi}{2} \frac{y}{Y_B} \right) dy$$

(4)

The differential light transmission due to the atomic and particulate matter is given by

$$\frac{dI}{d\lambda} = exp \left\{ -2 \sum_{i} \int_{o}^{y'} k_i \, dy \right\}$$

(5)

where: y' = minimum of Y_B and 198. 12 cm (the inside radius of the Calspan test facility.)

k_i = absorption coefficient due to either atoms, molecules, or particulates.

For atomic species, the absorption coefficient is given by

$$k_a = \frac{e^2 \lambda^4 f}{4 \pi m_e c^3} \frac{(\gamma_N + \gamma_c)}{(\lambda - \lambda_c)^2} \rho$$

(6)

where: e = 4.8032 x 10^{-10} esu
c = 2.9979 x 10^{10} cm/sec
m_e = 9.1055 x 10^{-20} gm
γ_N = $f g_m / 1.499 \lambda_c^2 g_n$
γ_c = $1.92 \sqrt{\frac{g_m}{g_{n_o}}} \frac{e^2}{m_e} \frac{\lambda}{c} f \rho$
λ_c = 3719.94 A for iron
f = 0.041 for iron

11

Substituting equation 6 into 5 and integrating over the pathlength Y_B gives optical transmission as a function of wavelength and number of atoms per unit axial length (dn/dx). Typical transmission for iron having a centerline density of 10^{16} atoms cm^{-3} and a radial expansion limit of 100 cm is shown in Figure 6; the curve labeled resonant absorption is an integrated computer solution of equation 5. The curve shows a typical linewidth of 0.85 Å at half height absorption. Superimposed on this resonant absorption is the measured entrance and exit slit function for the Jarrell-Ash monochrometer. The cross-hatched area is proportional to the number of photons that are detected. Computing these transmissions at various centerline densities and values of dn/dx gives sets of data that can be used to relate transmission to various values of dn/dx. A plot of such curves is shown in Figure 7. Transmissions are given for various values of dn/dx as a function of the radial expansion parameter, Y_B. Each experimental transmission measurement at 3719.94 Å can then be used to determine a value for the number of iron atoms in the expanding jet.

The monochrometer exit-plane detector configuration, which was used to compare particulate matter absorption and resonant absorption by iron atoms, is shown in Figure 8. Microscope cover slides were aluminized and placed so as to divide the photon flux from the Jarrell-Ash monochrometer into three photodetectors. Dumont type 6467 photomultiplier tubes were placed so as to detect the resonant absorption line (Photomultiplier #2), the continuum absorption over the adjacent 20 Å toward the ultraviolet (Photomultiplier #1) and the continuum absorption over the adjacent 20 Å toward the red (Photomultiplier #3). Prior to each experiment, a hollow cathode discharge lamp was used to adjust the center slit so as to have the 3719.94 Å iron resonant line exactly in the center of the middle exit slit. Each of these outputs is fed to recording oscilloscopes. Comparing the three recorded signals at known times enables a direct determination of preferential absorption due to free atoms and as well the velocity of the expanding jet relative to the particulates and the other explosively released products.

3.1   PARTICLE VELOCITY MEASUREMENTS

A series of shadowgraphs were taken in an attempt to obtain a relationship between the radial and axial velocities in the expanding jet. The photographic system included a high speed Graflex 1000 shutter-camera combination and a high power flashlamp. The flash duration was set at 1.5 microseconds. However, the open time of the Graflex shutter could not be reduced below about 10^{-3} seconds. Consequently, the light released due to the explosive detonation over the 10^{-3} seconds camera open time exceeded that due to the flashlamp and no meaningful measurements were obtained. The system has been modified to incorporate an image converter which enables effective camera shutter open times of 10^{-8} seconds, and hence the background light should be small. The infrared technique will be used in future studies.

Since a relationship between the axial and radial velocities is required to analyze the data, the velocity profiles from other similar investigations were used. Figure 9 was obtained from data published by Michel et al.[9] The radial velocity, $\overset{\circ}{Y}$, is shown as a function of the axial velocity, $\overset{\circ}{X}$. The two curves show the differences between a plane wave ($2\alpha = 180°$) system and a shaped charge ($2\alpha = 45°$) configuration. The velocity distribution for the latter (Figure 9b) was used to analyze the data presented in Section 5. The majority of our experiments were conducted using the metal confining techniques shown in Figure 4, and hence, the velocity distribution from a shaped charge system appears to best simulate the system studied.

Section 4

THEORETICAL PREDICTIONS

Several researchers have recently proposed equations-of-state for metals[11], [12], [13], [14] that are designed to relate measurable parameters to increases in system entropy, pressure, and temperature. The equation-of-state proposed and shown to fit the available experimental data by R. J. Naumann[15] is considered to be the most accurate at the present time. The analyses presented in this section are based primarily on Naumann's analytical model.

Consider a metal "A" that is traveling at a velocity w in free space. When this "flyer plate" strikes a "target" material "B", a shock wave is generated in "B", and a shock wave travels back through "A" up to the time it reaches the opposite boundary of each material. The shock waves travel away from the impact surface; hence, that part of the flyer plate "A" through which the shock wave has not passed is still traveling at the flyer plate velocity, w. The remainder of "A" has had the shock wave pass through it and has experienced a particle velocity jump equal to $w - u_{pA}$. Similarly, the target "B" has experienced a velocity jump equal to u_{pB} due to a shock wave passing through it. After being shock heated, the pressure, p, and particle velocities, u_{pA} and u_{pB}, are equal in both materials "A" and "B" and equal to their post shock values. Figure 10 was prepared using this impedance matching concept. The Hugoniot curves for the tantalum flyer plates used in these experiments were determined by plotting the velocity jump, $w - u_{pA}$, after shock passage based on the UCLA Hugoniot data. The Hugoniot curves for iron at the several porosities tested were obtained using Naumann's equation of state. The intersection point of the two curves for a given test condition determines the post shock particle velocity and pressure for a measured flyer plate velocity and target porosity. Thus, a direct relationship can be determined between flyer plate velocities and post shock particle velocities in the target material.

Substituting the correct equation-of-state for iron into the Hugoniot relation,

$$\mathcal{E}_1 (p_1 V_1) - \mathcal{E}_0 (p_0 V_0) = \frac{1}{2} (p_1 + p_0)(V_0 - V_1) \tag{7}$$

where: $\mathcal{E}$ = internal energy
V = volume
P = pressure
subscript "o" is the pre-shocked condition
subscript "1" is the post-shocked condition

allows direct calculation of the thermodynamic variables of the post-shocked material. Figure 11[15] is an example of the computer calculated results obtained using Naumann's equation of state. For a given post-shock pressure, the post-shock specific volume can be determined. The curves presented in the figure represent this relationship for the iron samples tested. The more porous the material (m = 1.72) the higher the post-shock pressure for a given relative volume V/V_0.

A relationship between post-shock particle velocity and system entropy can also be determined using Naumann's equation-of-state. This relationship is presented in Figure 12[15] as a function of initial target porosity. The less dense the target's initial structure, the greater the target's post-shock entropy, and hence, the higher its post-shock temperature.

The entropy added to the target can be determined through the use of Naumann's equation-of-state and the Hugoniot condition. The flyer plate velocity can be measured and used to determine the target's post-shock particle velocity and pressure. All other thermodynamic parameters are then calculable, and a series of curves can be constructed which will relate flyer plate velocity to final system entropy.

Once the target entropy is known, it can be used to determine the unloaded-system thermodynamic parameters. The unloading is an isentropic reduction in the target's pressure and temperature. By equating the target's post-shock entropy to that measured in a normally heated sample of iron, the iron temperature after being exposed to a vacuum can be determined.

Figure 13 presents the entropy for iron as a function of temperature according to the tabulation of Hultgren et al.[16] Each of the phase changes is shown in both the solid and liquid. The temperature and state of the unloaded iron target can be determined at the instant of shock unloading. The number of vapor atoms expected to be released from a droplet or disc of iron at a known temperature can then be calculated.

Alternatively, the vaporization can be measured as was done in these experiments, and a verification of the accuracy of this equation-of-state completed.

Section 5

SHOCK-HEATED IRON

Iron having porosities covering the range between 58% and 83% of normal crystalline densities were shock heated using the flyer plate method, and the degree of vaporization was measured in this experimental program. The iron matrix in the pre-shocked condition was studied using both a Bausch and Lomb Research Metalograph (resolution-limit~0.5 μ diameter particles) and an ETEC-Autoscan scanning electron microscope (SEM). Typical results using the light microscope are shown in Figure 14, and results for several surface areas and magnifications using the SEM are shown in Fig. 15. The advantages of the SEM are obvious and show that the matrix is composed of 2 to 5 μm dia. particles interspersed among a few large and a great number of smaller voids. The effects of "large" voids has not been determined; however, as will be shown, the measured vaporization is greater for porous samples than it is for normal density iron.

Normalized monochrometer signals, as measured for two of the twenty-two experiments completed during this program, are shown in Figures 16 and 17. The main difference between the two experimental configurations is the target plate thickness. Both target plates had a porosity of 58% normal iron density, were hit by a 0.13 mm thick tantalum flyer plate traveling at about 6 km/sec, used the Calspan-designed flyer launching system, and had a PBX 9404 H.E. main charge. The transmission curves are normalized outputs from the recorded oscilloscope signals of the three photomultiplier outputs. The signals are presented as a function of time after flyer plate impact on the target plate.

The transmission signal at the iron resonance wavelength is obtained by integrating Equation 5 to give

$$I_{Fe} = (I_{Fe})_o \ e^{(-2k'_a y')} \ e^{(-2k'_p y')} \tag{8}$$

17

where: I_{Fe} =   output from the photomultiplier monitoring the 3719.94 ± 1.5 Å iron resonant line.

Subscript "o" indicates no absorption

k'_a =   average value of absorption coefficient due to atomic iron over distance y' and at 3719.94 ± 1.5 Å.

k'_p =   average value of absorption coefficient due to particulates over distance y' and at 3719.94 ± 1.5 Å.

The transmission signal due to particulate matter at wavelengths longer and shorter than the iron resonant absorption line are given by

$$I_{lg} = (I_{lg})_o \ e^{(-2k''_p y')} \tag{9}$$

and

$$I_{sh} = (I_{sh})_o \ e^{(-2k'''_p y')} \tag{10}$$

where: k''_p =   average value of absorption coefficient at wavelengths longer than 3719.94 Å

k'''_p =   average value of absorption coefficient at wavelengths shorter than 3719.94 Å

respectively. Dividing the transmission signal at the iron resonance wavelength by that due to particulate matter, gives a measure of the absorption due to free iron atoms. Dividing Equation 8 by Equation 10 and assuming $k'''_p = k'_p$ gives

$$A_{Fe} = (A_{Fe})_o \ e^{(-2k'_a y')} \tag{11}$$

$$= (A_{Fe})_o \ I_{Fe} / I_{sh}$$

where: A_{Fe} =   the resulting transmission at 3719.94 Å if only free iron atoms were in the flowstream.

and I_{sh} and k_p''' are assumed equal to equivalent constants at 3719.94 Å.

Substituting these experimentally determined transmission characteristics into Eq. 5 gives a measure of the number of atomic iron atoms contained in the monochrometer's line of sight. The computed transmissions as a function of dn/dx is shown in Figure 7.

The physical extent of the vapor and particulate cloud is obtained through the use of shadow photography. The radius, Y_B, of this vapor cloud at the monochrometer's line of sight is given by

$$Y_B = \dot{y} t \qquad (12)$$

where: $\dot{y}$ = radial velocity of the vapor-particulate cloud as given by Figure 9b

t = time after flyer plate impact on the iron target plate.

the axial velocity of this cloud is given by

$$\dot{X} = d/t \qquad (13)$$

where: d = the distance from the target plate to the monochrometer line of sight, 231 cm.

The data presented in Figures 18 and 19 were obtained by a point-by-point calculation of the iron atom distribution as a function of the axial velocity, $\dot{X}$, for each of the target conditions used to obtain the data presented in Figures 16 and 17, respectively. Both configurations give about the same number of free iron atoms: 1.9×10^{22} atoms for the 0.76 mm thick target and 1.7×10^{22} atoms for the 1.02 mm thick target. However, the percentage vaporized is 75% for the thinner target as compared to 55% for the thicker one. Table III presents a summary of the data obtained by varying target and flyer plate properties as well as the method used to hold the H.E. and flyer plate.

19

Table III

EXPERIMENTAL RESULTS FOR SHOCK-HEATED IRON

Target Thickness, mm	Target Relative Density	Flyer Plate Thickness, mm	Flyer Plate Velocity, km/sec	# of Atoms Released	% Vaporization	Comments
0.76	58	0.13 mm	-------	-------	---	Free expansion PBX-9404
0.76	73	0.13	-------	-------	---	Free expansion PBXN-5
0.76	73	0.13	5-5.5	-------	---	Free expansion MPI
0.76	58	0.13	4.5-5.5	6.40×10^{21}	26.1	Free expansion PBX-9404
0.76	73	0.13	5-6	2.088×10^{21}	6.08	Free expansion PBX-9404
0.76	58	0.13	-------	3.33×10^{22}	133.3	Free expansion MPI
0.76	58	0.13	6-6.5	1.912×10^{22}	73.5	Contained PBX-9404
1.02	83	0.13	5-6	-------	---	Free expansion MPI
1.02	83	0.13	5-6	-------	---	Free expansion PBX-9404
1.02	83	0.25	6-6.5	6.96×10^{20}	1.36	Contained PBX-9404
1.02	58	0.13	-------	1.714×10^{22}	53.8	Contained PBX-9404
1.02	83	0.13	4	5.599×10^{21}	11.47	Free expansion PBX-9404
1.02	73	0.13	5-6	1.203×10^{22}	27.9	Free expansion PBX-9404
1.02	58	0.25	5-5.5	-------	---	Free expansion PBX-9404
1.02	58	0.13	-------	1.277×10^{22}	40.0	Free expansion MPI
1.02	58	0.13	5-5.5	9.164×10^{21}	28.9	Contained PBX-9404
1.02	58	0.13	5-5.5	7.455×10^{21}	22.9	Contained PBX-9404

20

Section 6
SUMMARY

A high altitude test chamber has been instrumented and used to test metal vaporization techniques. The main emphasis here was to find those techniques which provide fast and efficient energy coupling between the energy source and metal. Explosives were used to accelerate tantalum flyer plates to high velocities. These flyer plates produce strong shock waves in target metal plates upon impact. The net energy transfer has been shown to be sufficiently high to cause a 50 to 100% vaporization in porous iron. The techniques can be further refined and scaled to larger configurations.

REFERENCES

1. Davis, W. C., "Detonation Phenomena," University of California, Los Alamos Science Lab., March 1972.

2. Jones, O. E., "Metal Response Under Explosive Loading," Sandia Corporation, presented at the ASME Symposium, University of New Mexico, March 1972.

3. Johannson and Persson, Detonics of High Explosives, Academic Press, 1970.

4. Detonation Properties of Condensed Explosives Using the 13-K-W Equation of State, Los Alamos Science Lab., Report No. LA-2900 (1963).

5. Bullerdiek, W. A. - Unpublished Data

6. Kury, J. W., et al., "Metal Acceleration by Chemical Explosives," Lawrence Radiation Lab. Proc. of the 4th Symposium on Detonation, ACR-126, Office of Naval Research.

7. Kennedy, J. E., "Gurney Energy of Explosives: Estimation of the Velocity and Impulse Imparted to Driven Metal," Sandia Corporation Report SC-RR-70-790 (1970).

8. Hornung, K. and Michel, K. W., J. of Chem. Phys. 56 p. 2072 (1972).

9. Brunner, W., Föppl, H., and Michel, K. W., Astronautica Acta. 15 p. 613 (1970).

10. Huber, M. C. E. and Parkinson, W. H., Astrophysical Journal, 172 p. 229 (1972).

11. Naumann, R. J., Ph.D Thesis, University of Alabama 1970.

12. Naumann, R. J., NASA Report No. TN D-5892, 1970.

13. Ahrens, T. J., J. Applied Physics, 43 p. 2443 (1972).

14. Ahrens, T. J. and Urtiew, P. A., "The Use of Shock Waves in the Vaporization of Metals," Lawrence Radiation Laboratory, University of California, Livermore, California, n. d.

15. Naumann, R. J., J. Applied Physics 42 p. 4945 (1971)

16. Hultgren, R., Orr, R. L., Anderson, P. D. and Kelley, K. K., Selected Values of Thermodynamic Properties of Metals and Alloys, Wiley and Sons (1963).
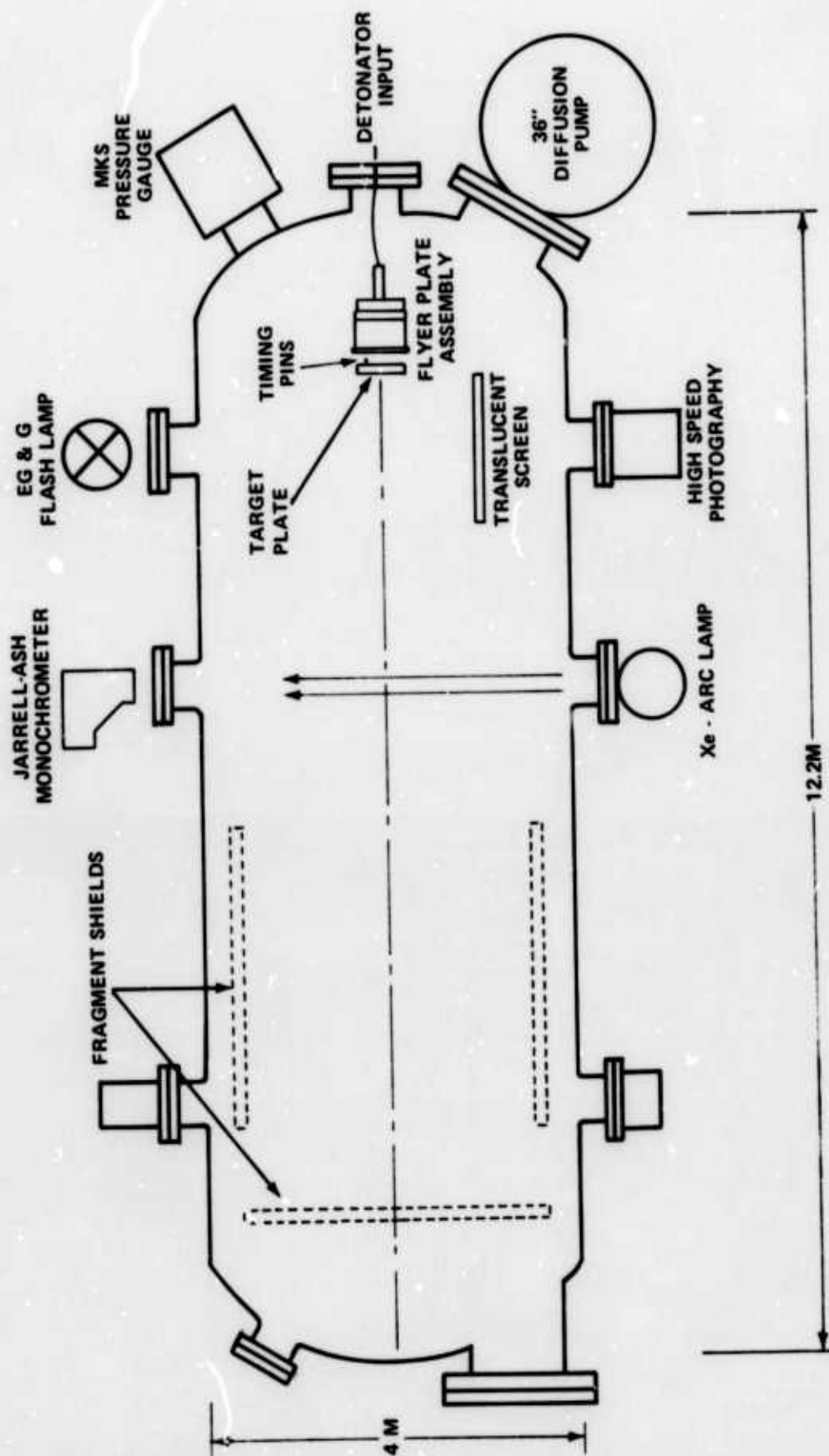
Figure 1 CALSPAN HIGH ALTITUDE METAL RELEASE TEST FACILITY

23
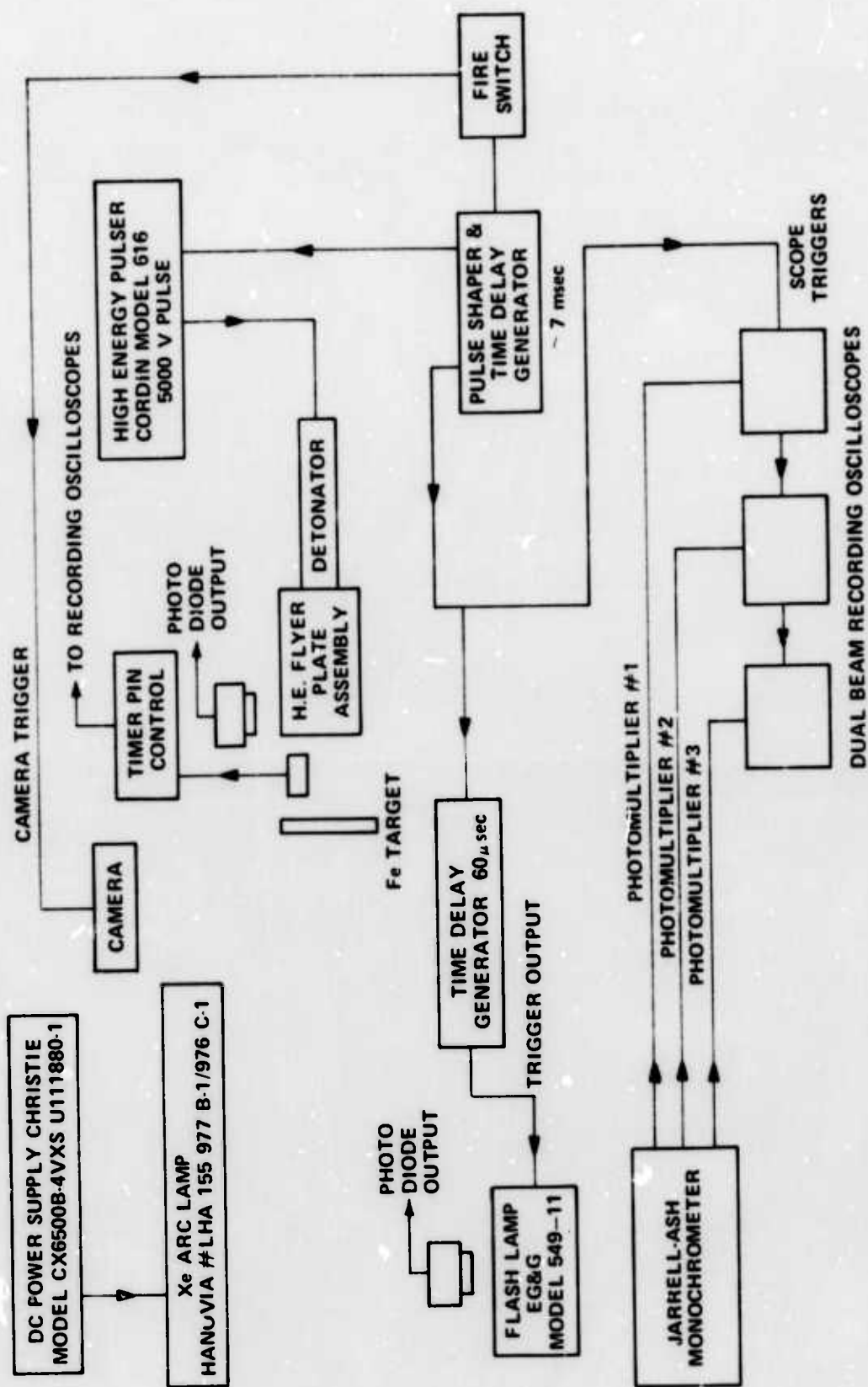
Figure 2   SYSTEM BLOCK DIAGRAM

1. REYNOLDS RP-87 EBW DETONATOR

2. DETONATOR HOLDER

3. DISTRIBUTOR PLATE, EXTRUSION LOADED
   W/EXTEX 8003 HIGH EXPLOSIVE

4. H.E. BOOSTER PELLET, PBX-9407

5. H.E. MAIN CHARGE W/ALTERNATE EXPLOSIVES

   PBX-9404

   PBXN-5

6. POLYACETATE FILM, 0.003" THICK x 1.2" DIA.

7. TANTALUM FLYER PLATE, 0.005" OR 0.010" x 1.2" DIA.
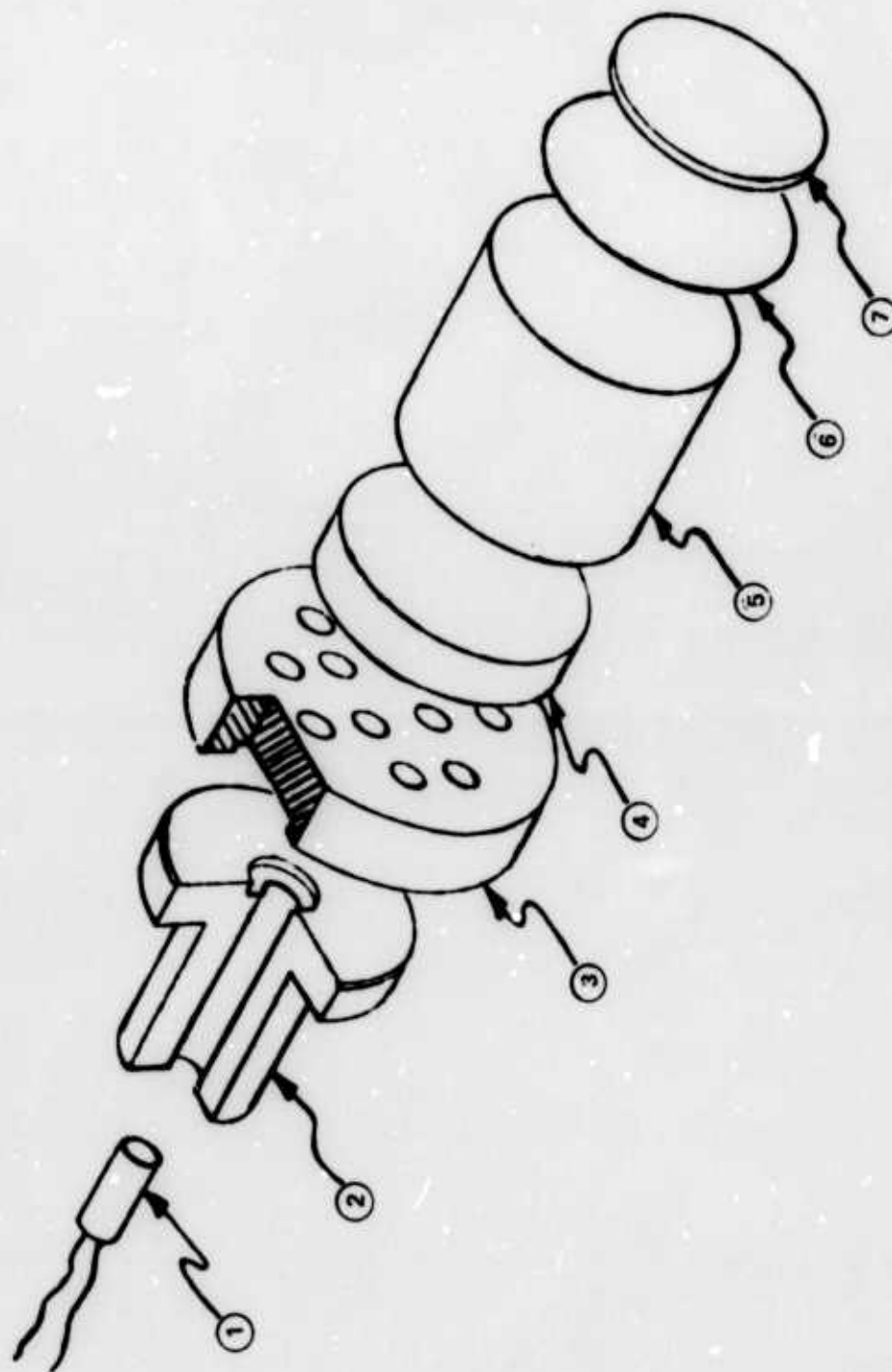
Figure 3   CALSPAN FLYER PLATE LAUNCH ASSEMBLY

25
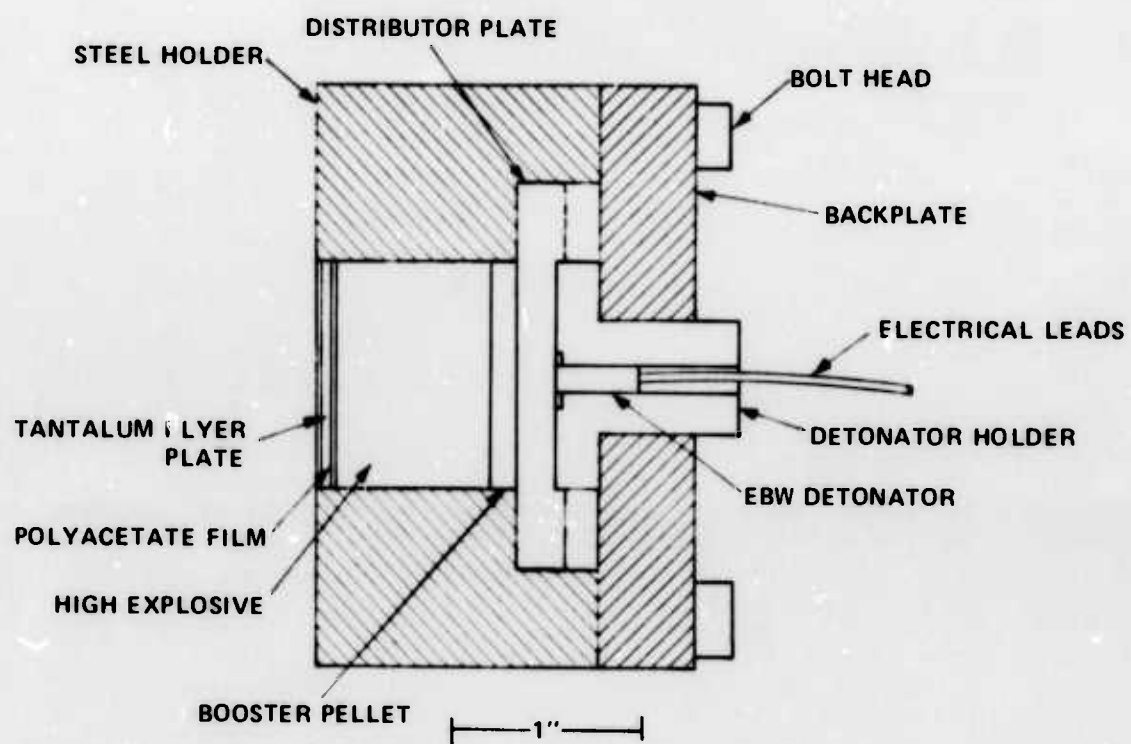
Figure 4 STEEL ENCLOSURE USED TO CONFINE DETONATION PRODUCTS

26
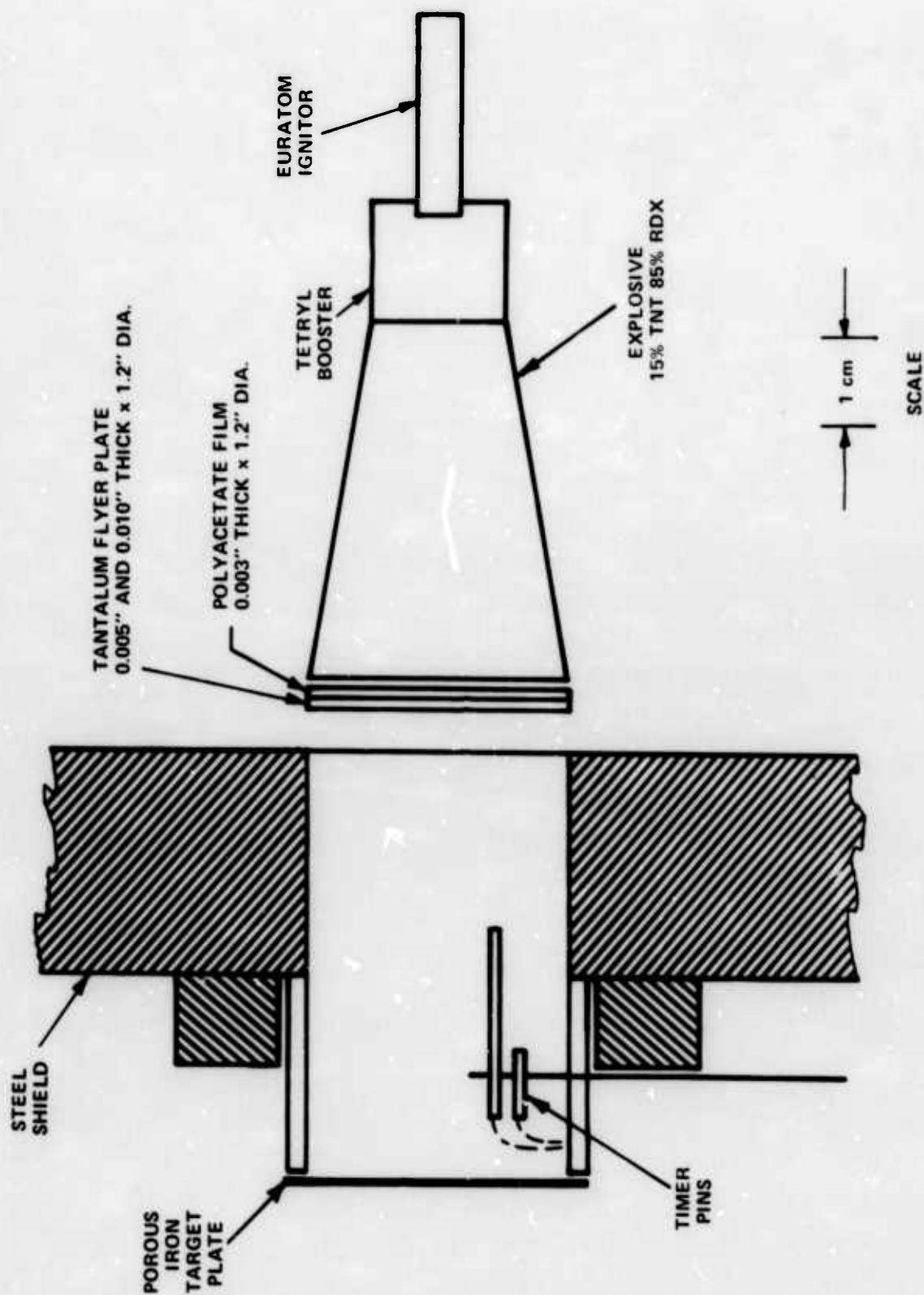
Figure 5 FLYER PLATE LAUNCH ASSEMBLY AS DESIGNED AND USED AT THE MAX-PLANCK-INSTITUT
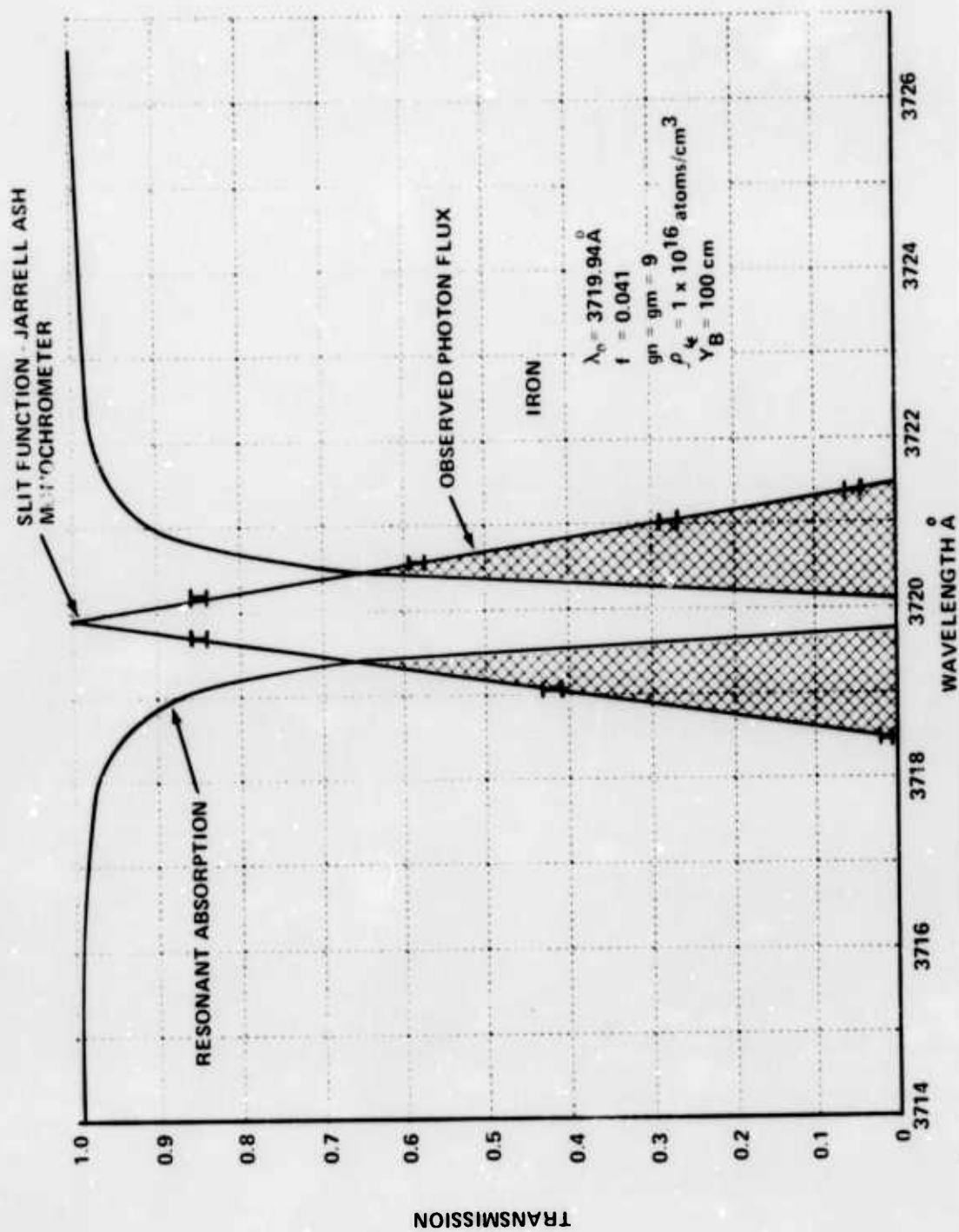
Figure 6 PRESSURE BROADENED ABSORPTION

28
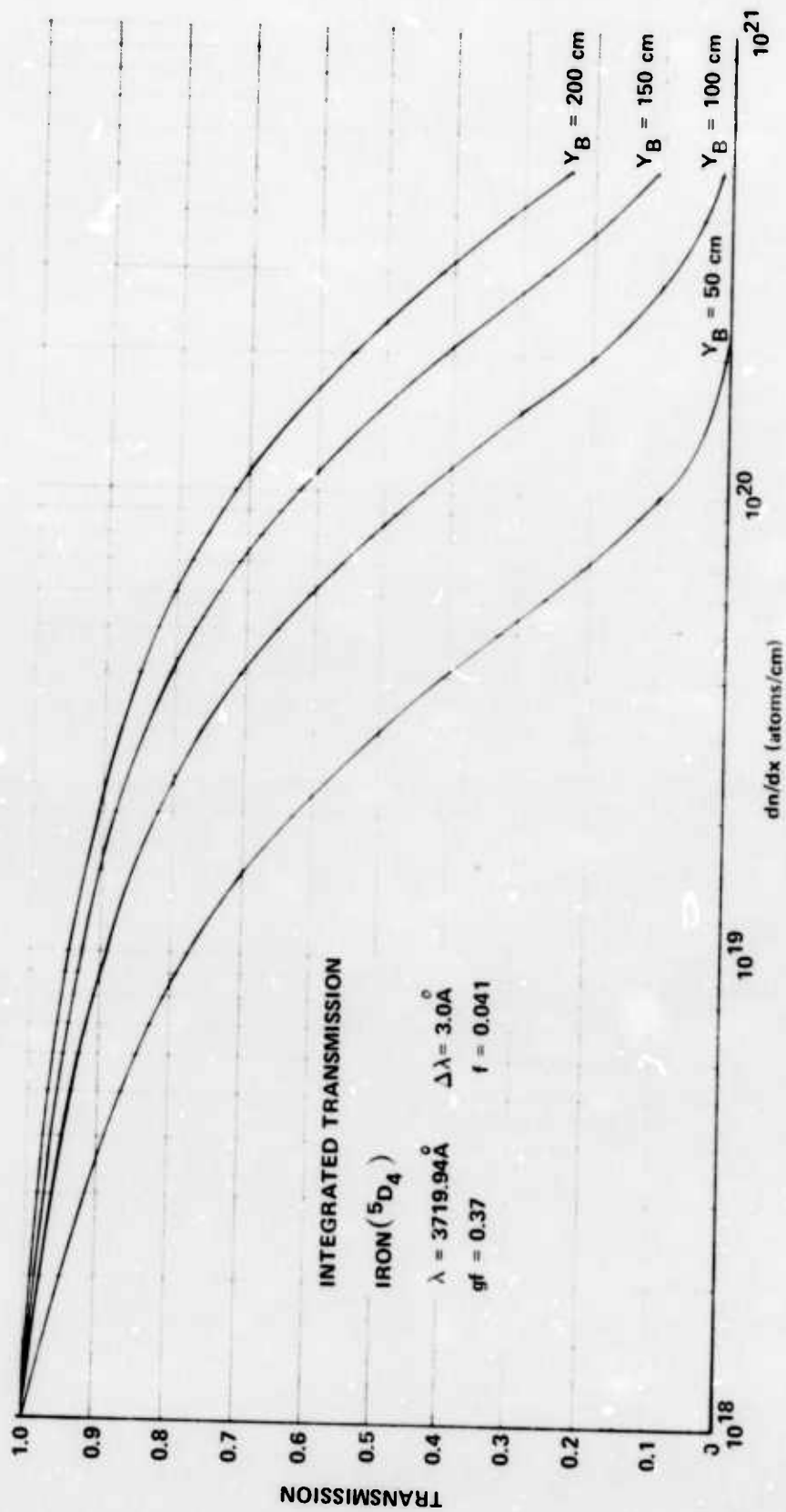
Figure 7 INTEGRATED TRANSMISSION

INTEGRATED TRANSMISSION

IRON($^5D_4$)

$\lambda = 3719.94\text{Å}$ $\Delta\lambda = 3.0\text{Å}$

$gf = 0.37$ $f = 0.041$

$Y_B = 200$ cm
$Y_B = 150$ cm
$Y_B = 100$ cm
$Y_B = 50$ cm

dn/dx (atoms/cm)

TRANSMISSION

29
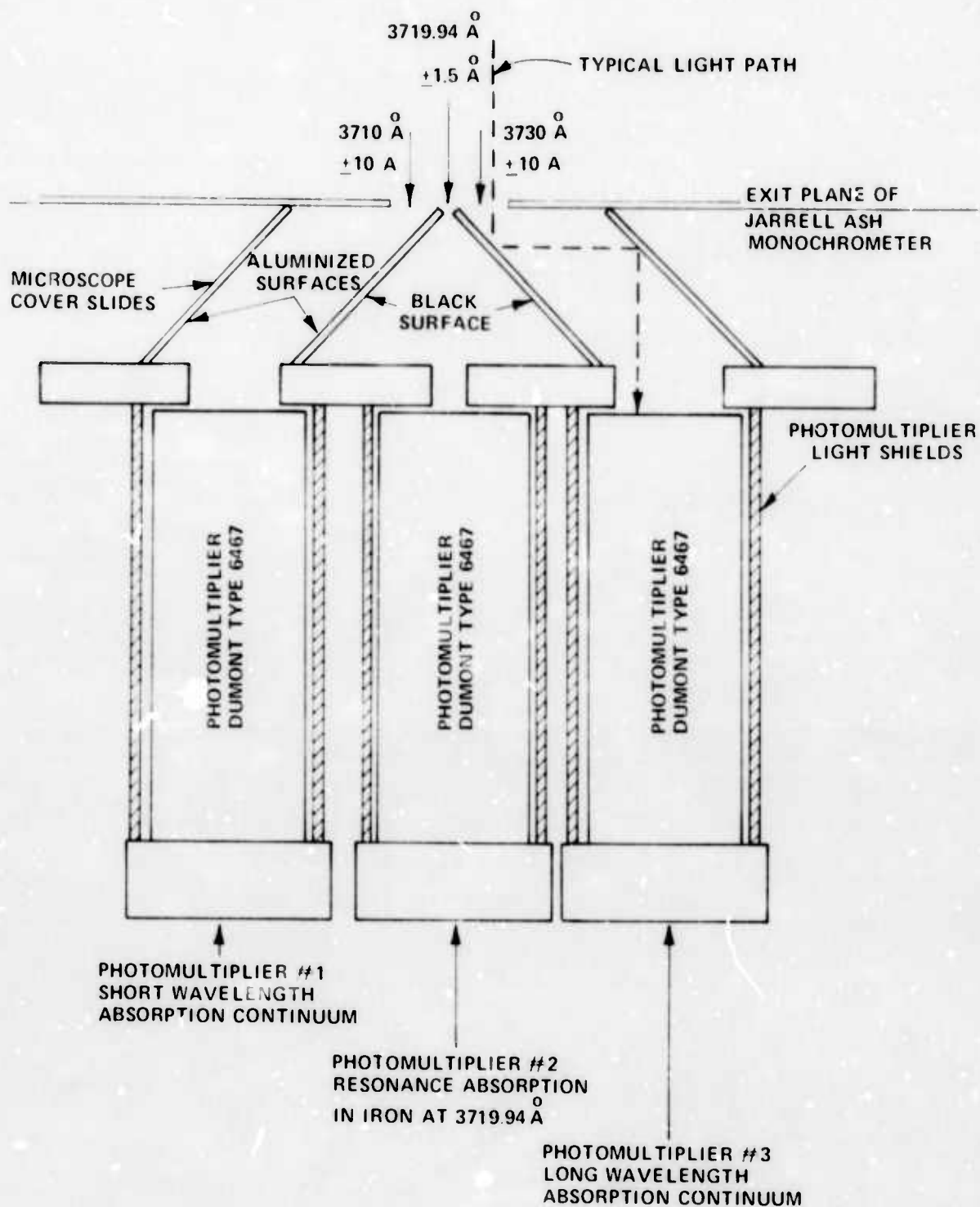
Figure 8   MONOCHROMETER EXIT-PLANE DETECTOR CONFIGURATION

(a) $2\alpha = 180^{\circ}$

(b) $2\alpha = 45^{\circ}$
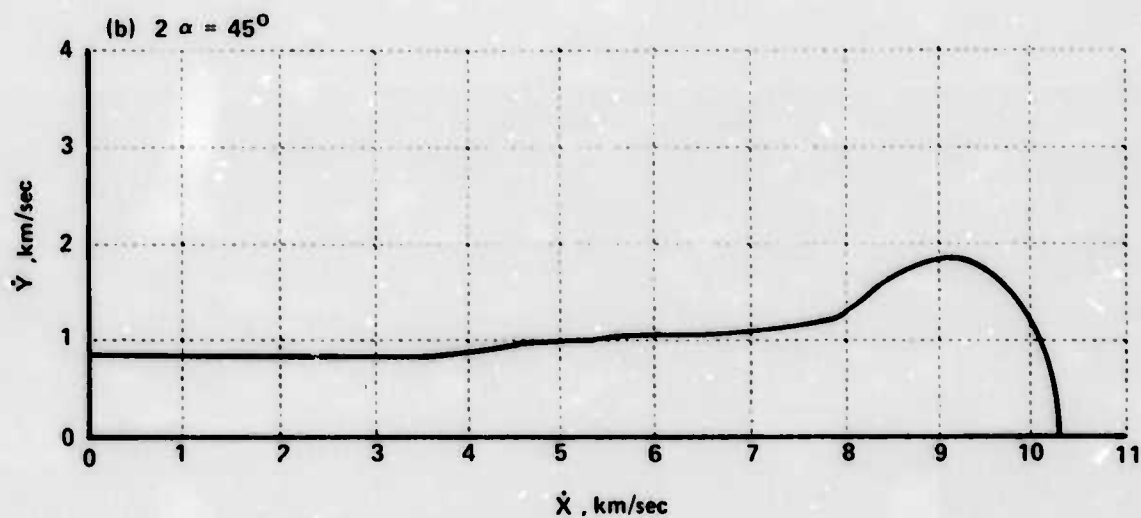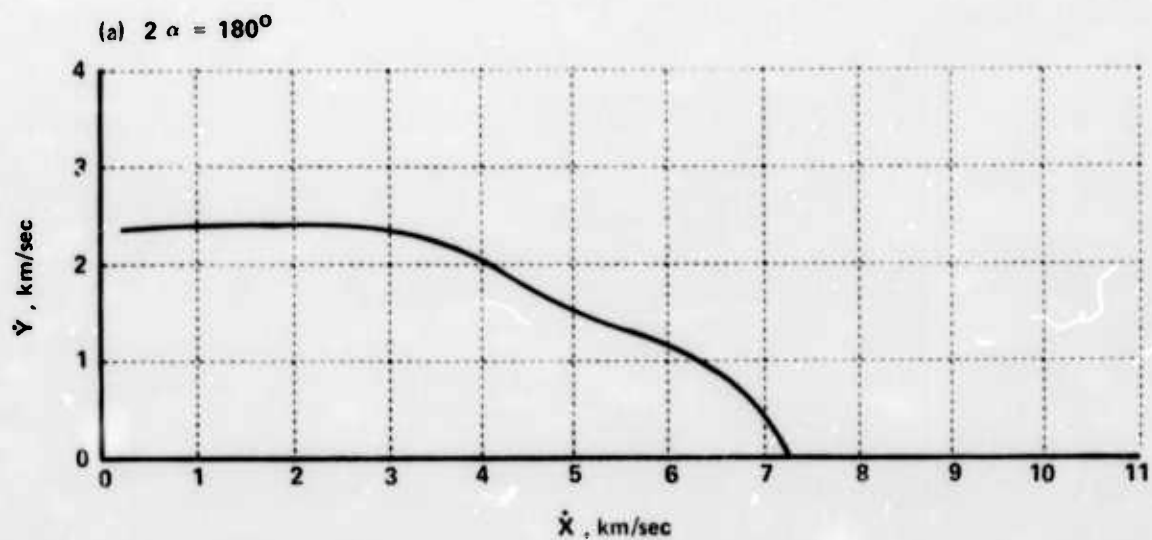
NOTE: DATA OBTAINED FROM REFERENCE 9.

Figure 9   DISTRIBUTION OF VAPOR ATOMS OVER FORWARD VELOCITY, $\dot{X}$, AND RADIAL COMPONENT, $\dot{Y}$, AS MEASURED AT THE MAX-PLANCK-INSTITUT α IS THE ANGLE OF THE H.E. CHARGE OUTPUT FACE WITH RESPECT TO THE CHARGE AXIS OF REVOLUTION

31
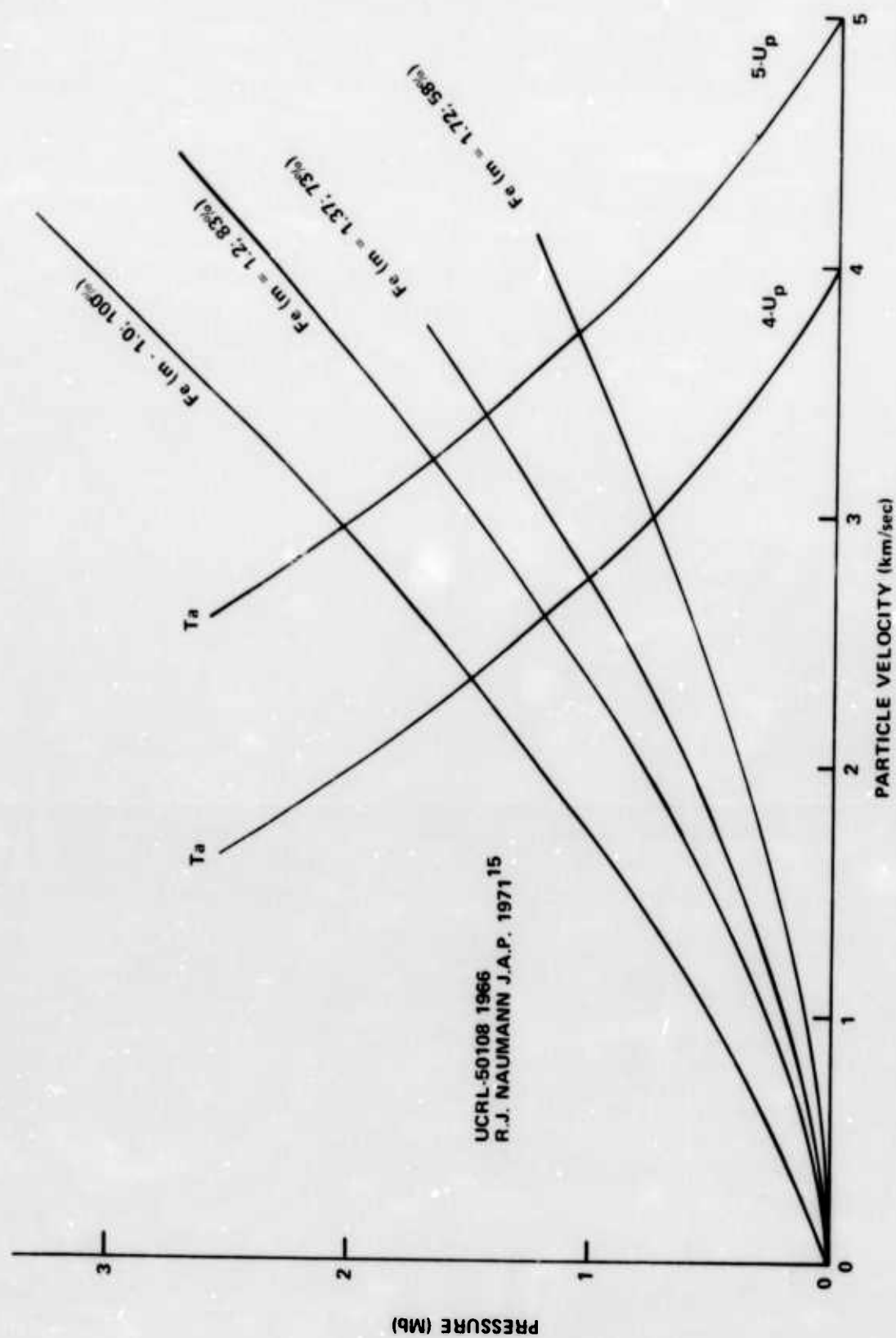
Figure 10   IMPEDANCE MATCHING FOR Ta FLYER ON Fe TARGET

UCRL-50108 1966
R.J. NAUMANN J.A.P. 1971[15]

32
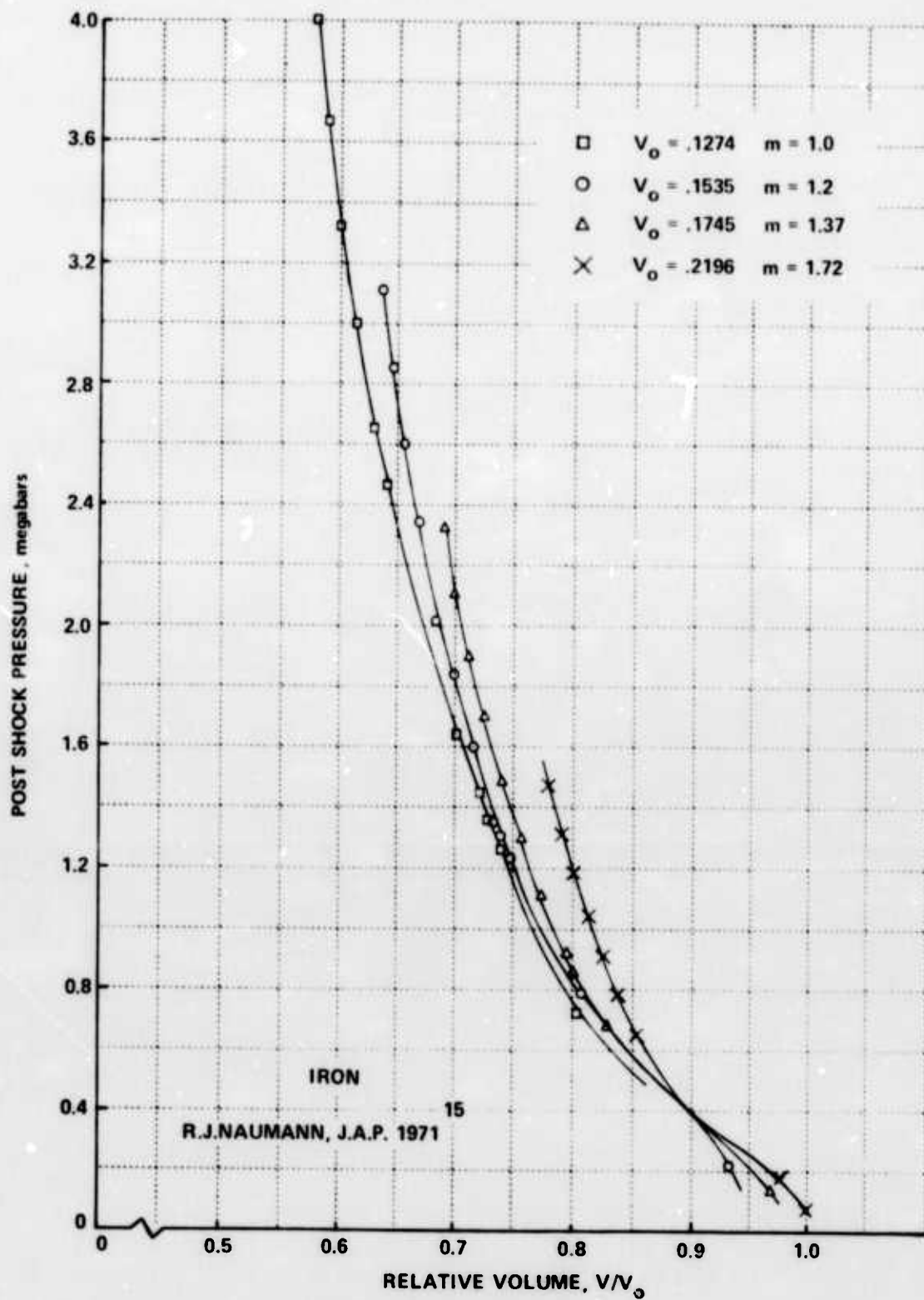
Figure 11 P-V DIAGRAM FOR IRON HAVING VARIOUS INITIAL SPECIFIC VOLUMES, V_o.
THE DISTENTION RATIO, m, IS GIVEN FOR THE PRE-HEATED SAMPLE

33
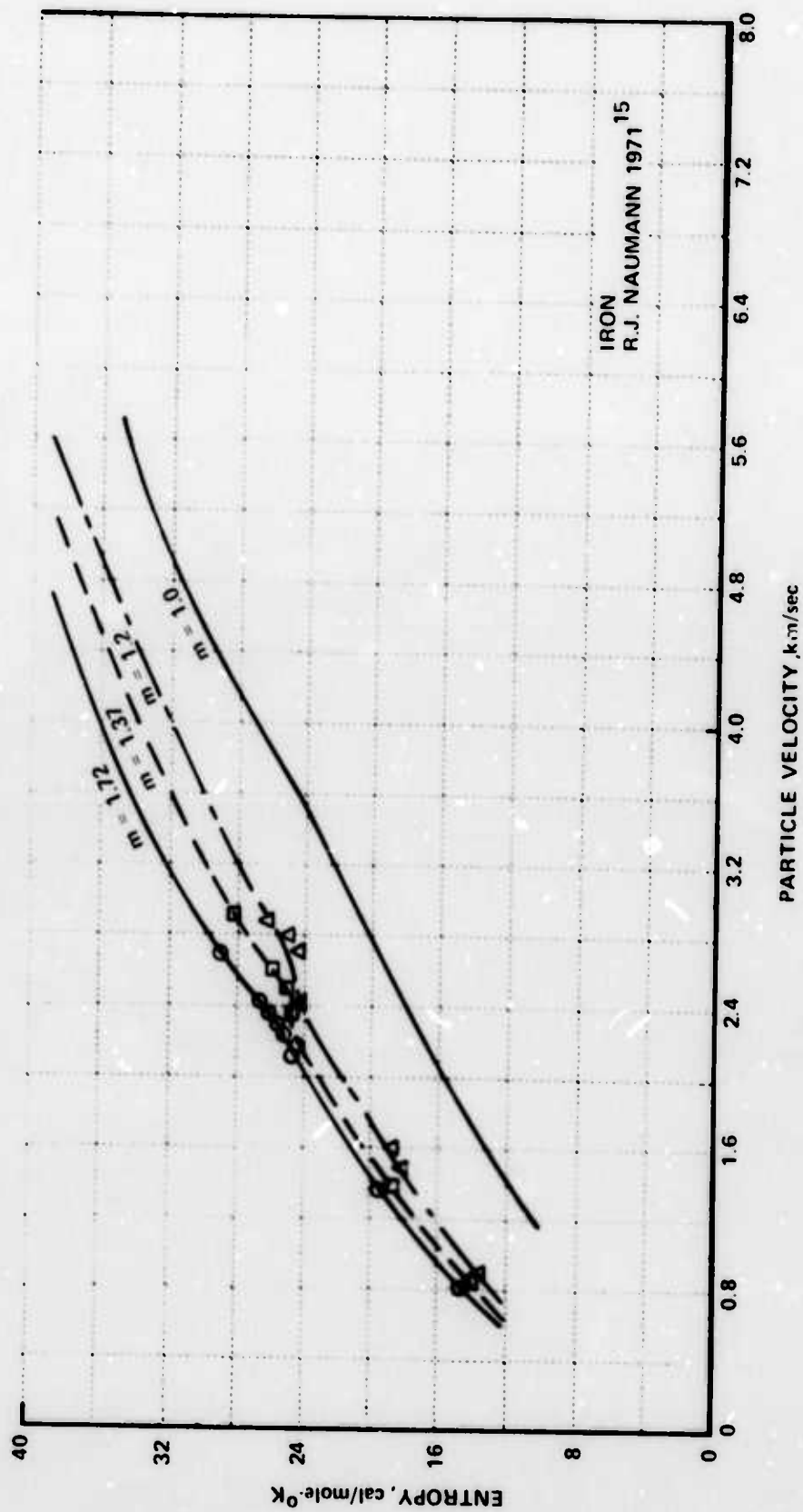
Figure 12 ENTROPY OF POROUS IRON AS A FUNCTION OF PARTICLE VELOCITY

3-4
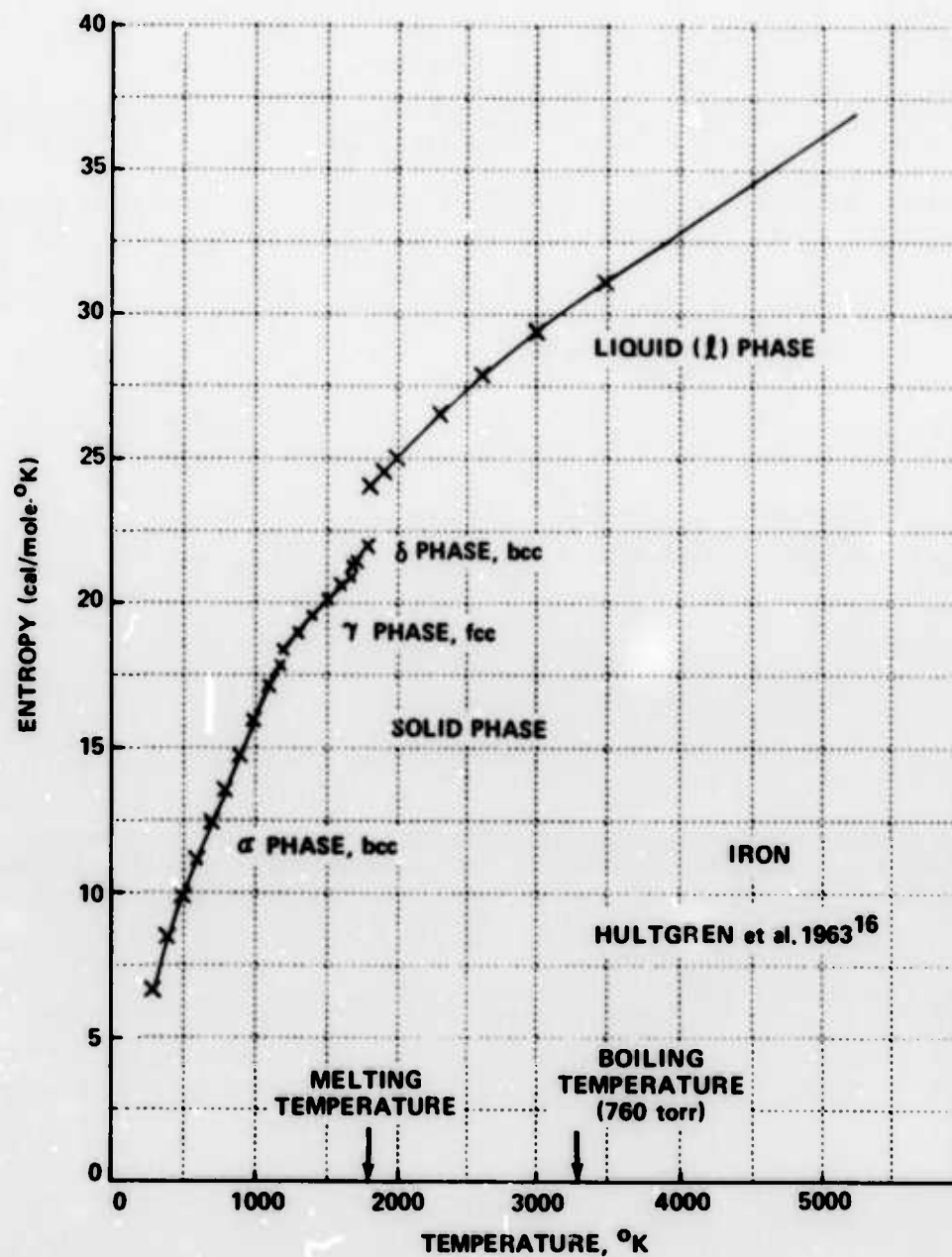
Figure 13 ENTROPY AS A FUNCTION OF TEMPERATURE FOR NORMAL CRYSTALLINE IRON
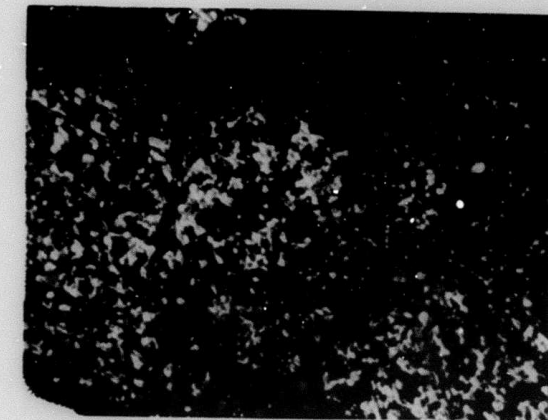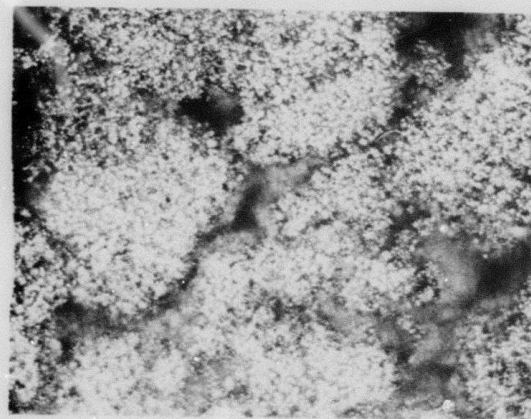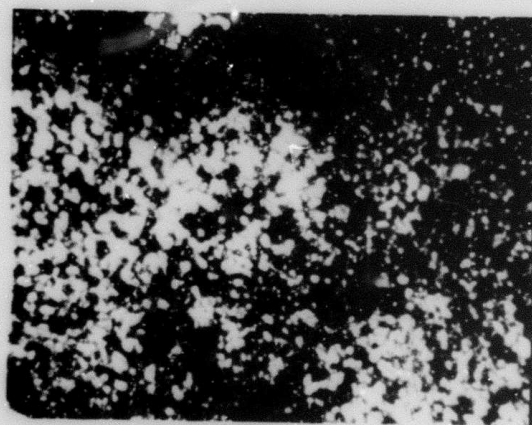
Figure 14   POROUS IRON SPECIMEN - 58% NORMAL DENSITY
LIGHT MICROSCOPY

10μ

10μ

100μ

$\dashv$ 10μ $\vdash$

$\dashv$ 1μ $\vdash$
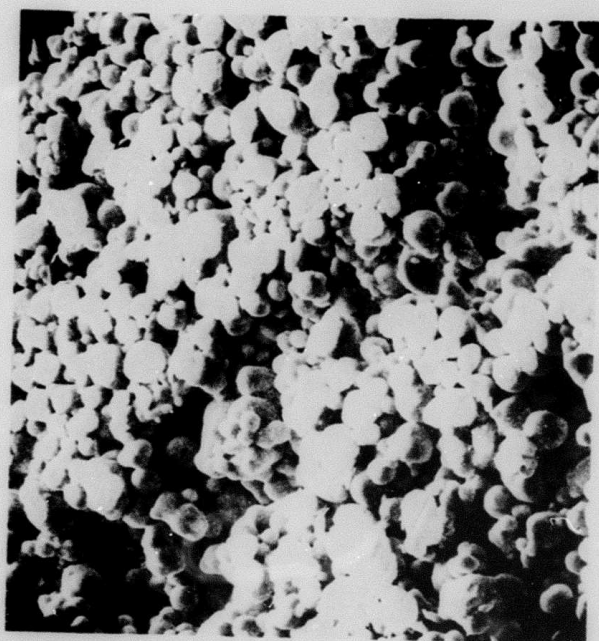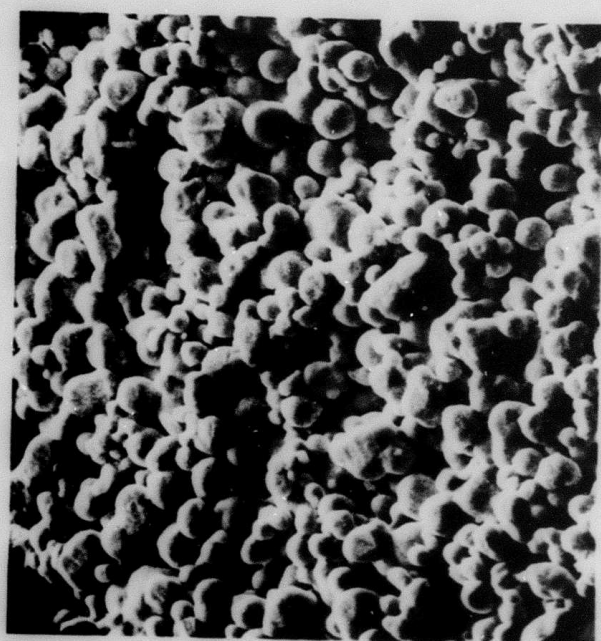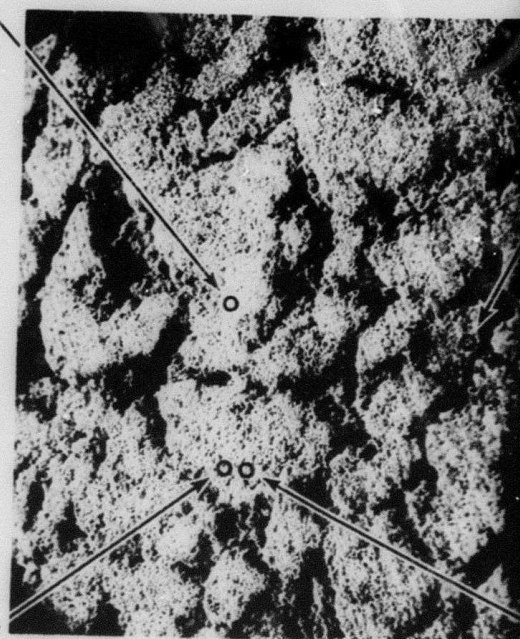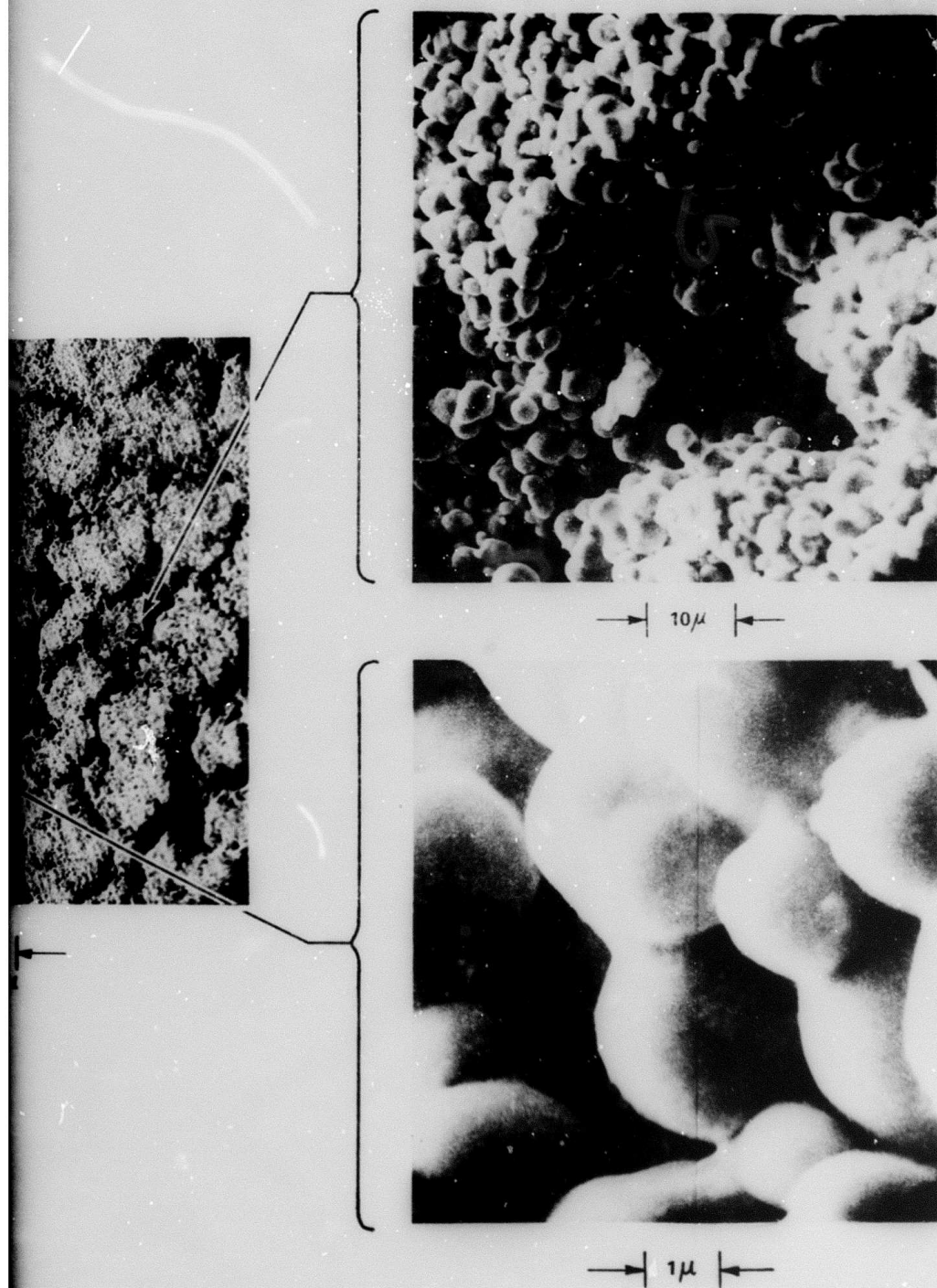
Figure 15   POROUS IRON SPECIMEN - 58% NORMAL
DENSITY SEM DIAGNOSTIC

37
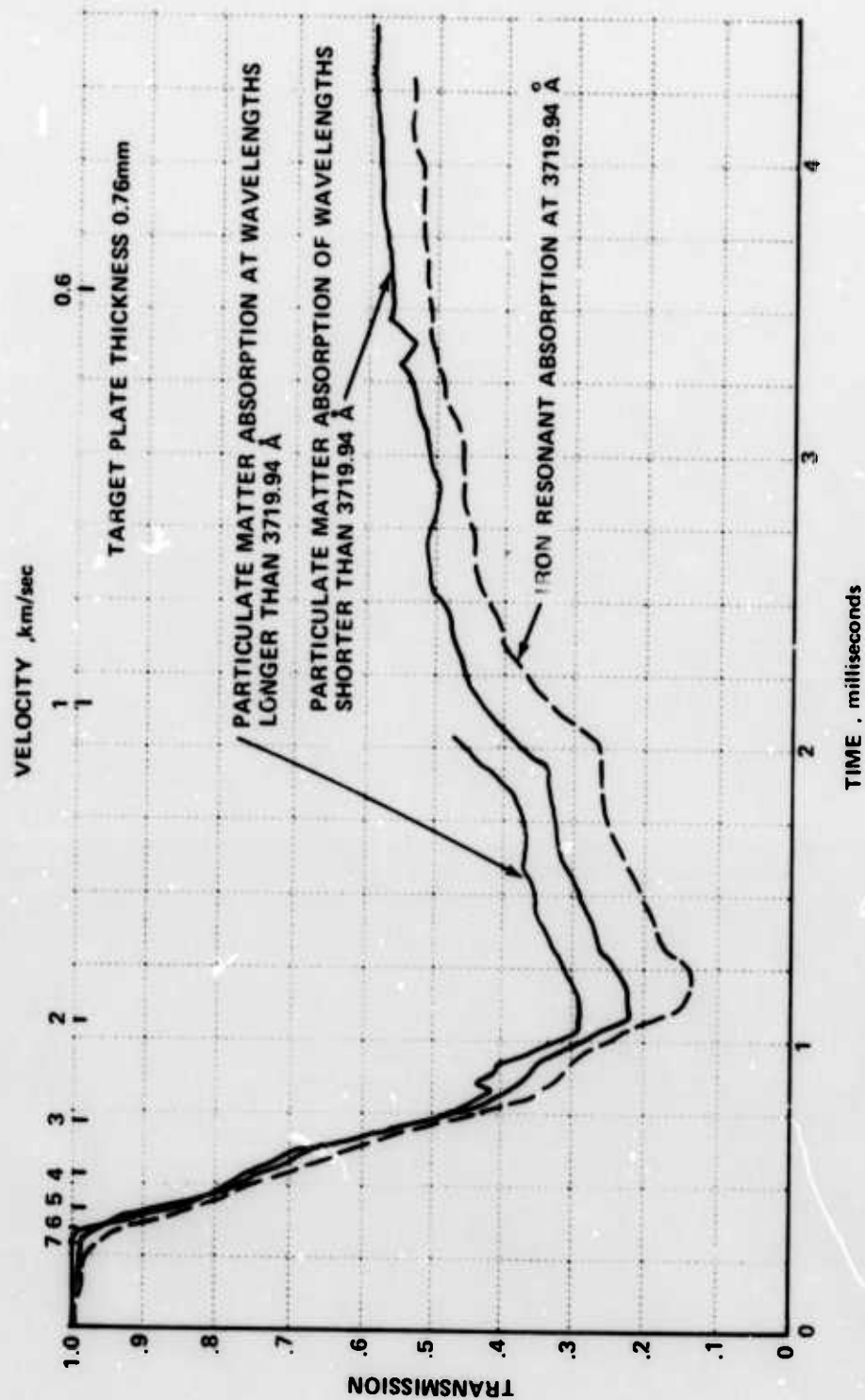
Figure 16   MONOCHROMETER SIGNALS SHOWING IRON VAPORIZATION

38

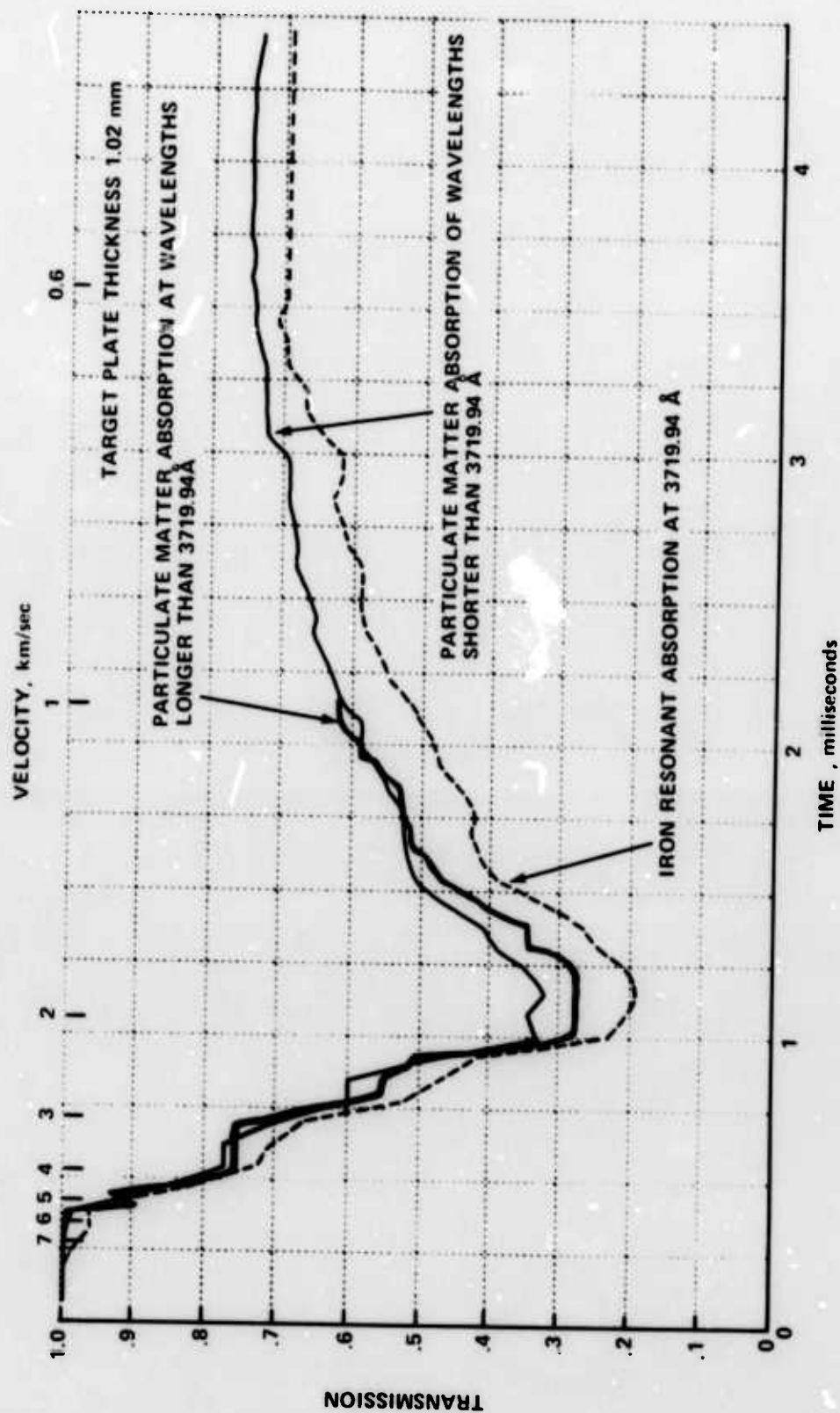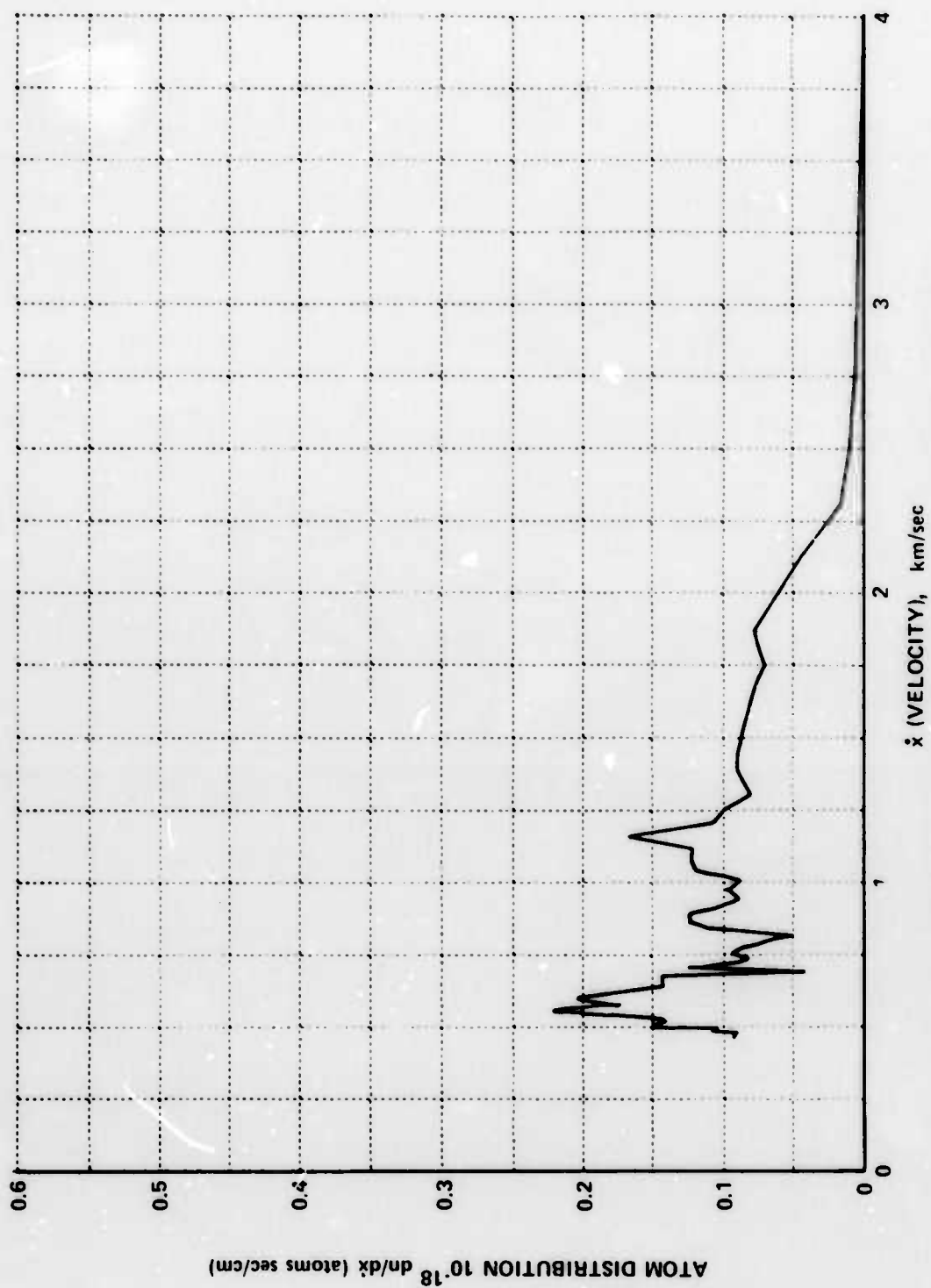Figure 17   MONOCHROMETER SIGNALS SHOWING IRON VAPORIZATION

Figure 18   IRON ATOM DISTRIBUTION OVER ITS FORWARD VELOCITY Ẋ
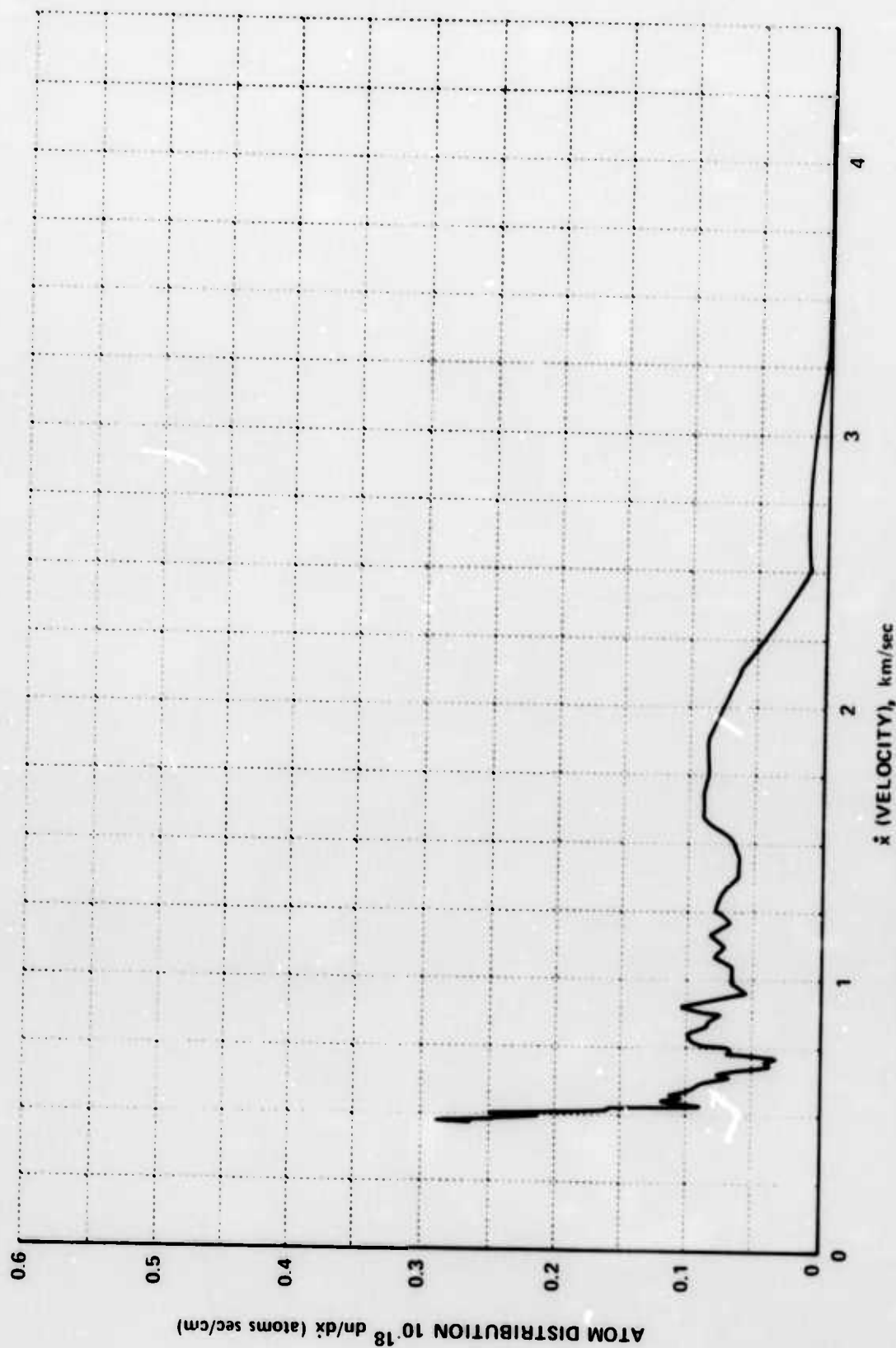TARGET THICKNESS 0.76 mm, POROSITY 58%

40

Figure 19   IRON ATOM DISTRIBUTION OVER ITS FORWARD VELOCITY Ẋ
TARGET THICKNESS 1.02 mm, POROSITY 58%